The Multiple-Vortex Structure of a Tornado

Joshua Wurman

School of Meteorology, The University of Oklahoma, Norman, Oklahoma

ABSTRACT

The structure and behavior of multiple subtornadic-scale vortices in a tornado were examined and were compared with laboratory, conceptual, and numerical models. Unique radar observations of an exceptionally large and violent tornado obtained with a Doppler on Wheels mobile radar on 3 May 1999 in northern Oklahoma provided the opportunity, for the first time ever with quantitative radar measurements, to characterize the size, strength, motion, horizontal and vertical structure, and persistence of multiple vortices in a tornado. Doppler velocity, received power, and spectral-width data were used to study the vortices. The structures of the multiple subtornadic-scale vortices were similar to that of tornadic vortices in certain respects. They exhibited doughnut-shaped received power maxima and/or hooks surrounding comparatively clear central eyes. Doppler velocity differences across the vortices decreased with height. However, the vortices exhibited intense small-scale shears at their centers that could not be explained by the inability to resolve core flow regions adequately. Even though the distances between wind speed maxima were typically about 250 m, approximately one-half of the total shear in most vortices was concentrated across 50 m or less. This was in contrast to the approximately solid-body rotation exhibited in the core flow region of the parent tornado. It is hypothesized that either the very rapid motion of the vortices or small-scale transient updrafts caused this phenomenon. The shear across the vortices, about 100 m s^{-1}, was about one-half of the total shear across the tornado, about 170 m s^{-1}. The amplitude of the vortices was consistent with some, but not all, numerical and laboratory predictions. The central shear regions of the vortices exhibited estimated vertical vorticities of 4–8 s^{-1}, the highest ever observed in tornadic flows. Wind speed changes of 50 m s^{-2}, corresponding to 5 times the acceleration of gravity, would have been experienced by stationary observers impacted by the multiple vortices. The vortices appeared to translate around the tornado at a fraction of the peak azimuthally averaged tangential velocity of the parent tornado, consistent with some theoretical and computational predictions. It was not possible to rule out, however, that, in the absence of any upstream propagation, the vortices merely translated at the peak azimuthally averaged tangential velocity of the parent tornado at the radius of the vortices as predicted in other studies. Individual vortices were trackable for at least 40 s, revolving at least 180° around the parent tornado. The multiple vortices were most prominent during the weakening phase of the tornado, as peak azimuthally averaged tangential winds dropped from over 80 to less than 70 m s^{-1}, and just after the radius of the peak flow region had contracted somewhat, possibly indicating changes in the swirl ratio.

1. Introduction

Conceptual models of tornado structure predict that, under certain conditions, a primary tornado vortex will break down into several subtornadic scale multiple vortices (hereinafter ''multiple vortices''; Davies-Jones 1976; Rotunno 1978; Snow 1978; Staley and Gall 1979; Gall 1983). Computer simulations (Walko and Gall 1984; Rotunno 1977, 1979, 1984; Lewellen 1993; Lewellen et al. 1997; Fiedler 1998) and laboratory simulations (Ward 1972; Church et al. 1979; Church and Snow 1993) have also reproduced multiple-vortex structure.

Multiple vortices have been observed visually and in patterns of damage for decades (Fujita 1970; Agee et al. 1975, 1977; Pauley and Snow 1988). Direct radar evidence of subtornado-scale wind maxima probably associated with multiple vortices was first obtained in a large tornado that destroyed much of the small town of Spencer, South Dakota, in 1998 (Wurman 1999), producing damage rated F4. The tornado was observed by a Doppler on Wheels radar (discussed below) at a range of as little as 1.7 km to the center of circulation. In that tornado, the several observed vortices were substantially weaker than the primary tornadic flow, superimposing perturbations of approximately 20–30 m s^{-1} on a tor-

Corresponding author address: Joshua Wurman, 1945 Vassar Circle, Boulder, CO 80305.
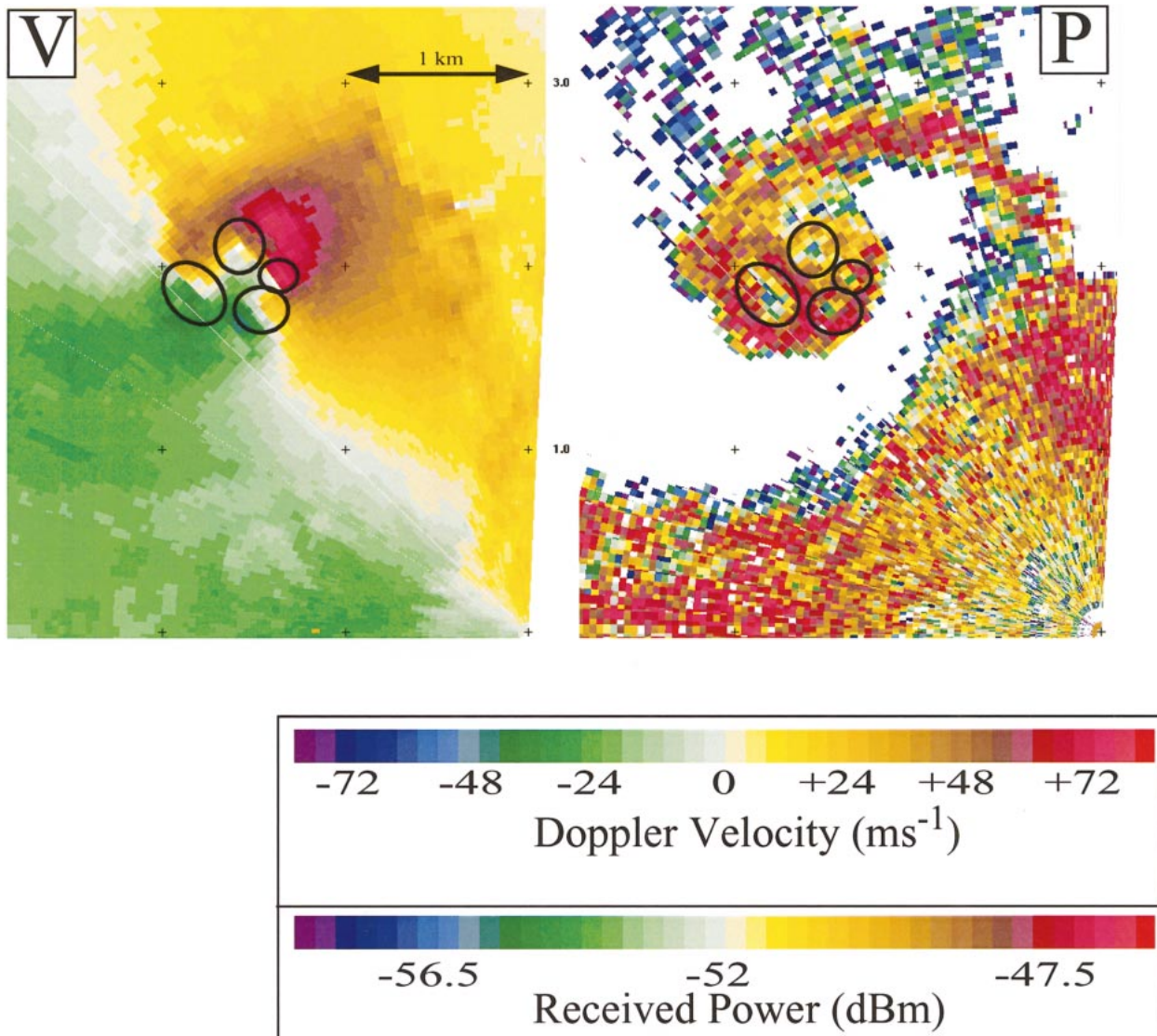E-mail: jwurman@ou.edu

FIG. 1. (left) Doppler velocity and (right) received power fields in the Spencer, SD, tornado of 30 May 1998 (0136 UTC 31 May 1998). Intense shear zones and power minima indicate location of multiple vortices, the first ever observed by radar. Ovals delimit regions of very high shear and power minima. Tick marks are shown every kilometer here and in all plots of DOW data in this paper, unless otherwise indicated. This and all radar images in this paper have been rotated so that north points toward the top of the page. The tornado was approximately 3 km from the radar. The radar beam crossed through the tornado at about 250 m AGL.

nado-relative flow of approximately 85 m s^{-1} (Fig. 1). The primary tornado vortex had a core diameter (distance from peak inbound to peak outbound Doppler wind speeds) from approximately 500 m at 250 m AGL to 700 m at 1000 m AGL. So, multiple vortices revolving around the tornado at 0.5–1.0 times the peak tornadic wind speed (see propagation speed discussion below) would have completed circuits in 10–20 s. Because the radar scanned through the tornado every 6 s, it was impossible to track the continuity of the vortices, their motion, or vertical structure. The vortices caused a degradation of the typical clear eye structure observed frequently in received power data (Wurman and Gill

2000, hereinafter WG; Burgess et al. 2002, hereinafter B) obtained in tornadoes not exhibiting strong multiple vortices. At certain times, several smaller low-received-power "eyes" were evident.

Subsequent observations from a 3-mm-wavelength mobile radar revealed evidence of multiple vortices in one of the tornadoes that occurred during the 3 May 1999 Oklahoma tornado outbreak (Bluestein and Pazmany 2000). They observed wind field reversals and perturbations to the received power field probably associated with multiple vortices in individual slices through the tornado.

Until recently, however, quantitative, three-dimen-

FIG. 2. A DOW mobile radar. The 2.44-m-diameter antenna produces a 0.93° beam and can scan at speeds up to 60° s⁻¹. The leveling and stabilization system provides a stable platform in high winds that can be leveled with an accuracy of about 0.2° within about 40 s. The operator cabin to the rear of the truck cab encloses transmitting, receiving, signal processing, navigational, antenna control, and other hardware.

sional, fast, radar observations permitting a detailed characterization and mapping of the structure, motion, and behavior of multiple vortices have been nonexistent.

2. Radar, site, and data description

a. DOW radar description

The Doppler on Wheels mobile radars (DOWs; Wurman et al. 1997; Wurman 2001) have been developed for the express purpose of obtaining high-resolution data in tornadoes and other small-scale and short-lived phenomena. One of the DOWs is shown in Fig. 2. The DOWs have undergone considerable upgrading since the prototype DOW1 was deployed in 1995 (Wurman 2001). The DOWs can scan rapidly, up to 60° s⁻¹; produce transmit pulses of less than 130 ns; and sample signals every 83 ns to obtain oversampled range resolution of 12.5 m and nonoversampled resolution of about 20 m. Staggered-pulse-repetition-frequency transmit modes virtually eliminate velocity ambiguities in all but the strongest tornadoes, as discussed below. Real-time displays of Doppler velocity and reflectivity, using updated National Center for Atmospheric Research (NCAR) Personal Computer–Integrated Radar Data Acquisition System (PIRAQ-2) signal processing hardware, as well as rapid deployment and undeployment ability, are tailored for tornado intercept efficiency and safety. The DOWs operate at approximately 9.375 GHz, with peak transmitted power of 250 kW, and 2.44-m parabolic antennas produce beamwidths of 0.93°. At 1.5 km, typically the minimum safe deployment range from the center of *large* tornadoes, these characteristics result in sample volumes of as small as 24 m × 24 m × 12.5 m (7200 m³). Near weaker and smaller tornadoes, data with beamwidths as low as 3 m have been obtained, at ranges of as low as 30 m to the edge of the core flow regions.

The DOWs have resolved the structure and evolution of several tornadoes with single- and dual-Doppler measurements (WG; Wurman et al. 1996a,b; Wurman 1999; Richardson et al. 2001; B). However, they are only marginally suited to resolving extremely small-scale features such as typical tornadic multiple vortices because the scale of these vortices or "suction spots" has been inferred as being as small as 10 m (Fujita 1970). Ultra-high-resolution radars employing 3-mm-wavelength transmissions with beamwidths as low as 0.19° can obtain data at much finer azimuthal scales [Bluestein et al. (1993, 1995); Bluestein and Pazmany (2000); with 5-m beamwidth at 1.5-km range and true range resolution of 30 m resulting from 200-ns transmit pulses, volumetric resolution at 1.5 km is 750 m³, nearly 10 times as fine as the DOWs], *perhaps* permitting the limited observation of 10-m scale phenomena (1000 m³). Existing short-wavelength radars lack the ability to scan rapidly, penetrate deeply into heavy precipitation and debris, or perform practical dual-Doppler coordination, however. A multibeam rapid-scan DOW, which is now under development by the University of Oklahoma and NCAR (Wurman and Randall 2001), will be deployed as early as 2003 and will offer the ability to complete volumetric scans in as little as 5–10 s. With volumetric updates this frequent, observation of the temporal evolution of large multiple vortices may become possible. However, neither the existing or proposed rapid-scan DOWs nor existing short-wavelength radars can collect data with resolution fine enough to resolve accurately 10-m scales of motion (Carbone et al. 1985). In exceptional circumstances, however, such as those described below, the existing DOWs can resolve multiple-vortex structure and behavior.

b. Storm overview

On 3 May 1999, several dozen tornadoes occurred over Oklahoma and Kansas (Speheger et al. 2002). At least seven of these were observed from close range by the DOW radars, including those occurring near the towns/cities of Apache, Cement, Chickasha, Bridge Creek–Moore–Oklahoma City, Spencer, Jones, and Mulhall, Oklahoma. At 0310 UTC 4 May 1999 (2210 local time 3 May 1999), a supercell thunderstorm [storm B in Speheger et al. (2002)] moved northeastward through northern Oklahoma. The KTLX Weather Surveillance Radar-1988 Doppler (WSR-88D) in Norman, Oklahoma was able to observe the storm from an approximately 85-km range (Fig. 3), and a pronounced hook echo and intense cyclonic circulation were documented.

This thunderstorm produced an exceptionally large and powerful tornado that was observed by the DOW from 0310 to 0328 UTC from a stationary deployment. Observations were collected earlier while the DOW was moving toward the deployment site and afterward while
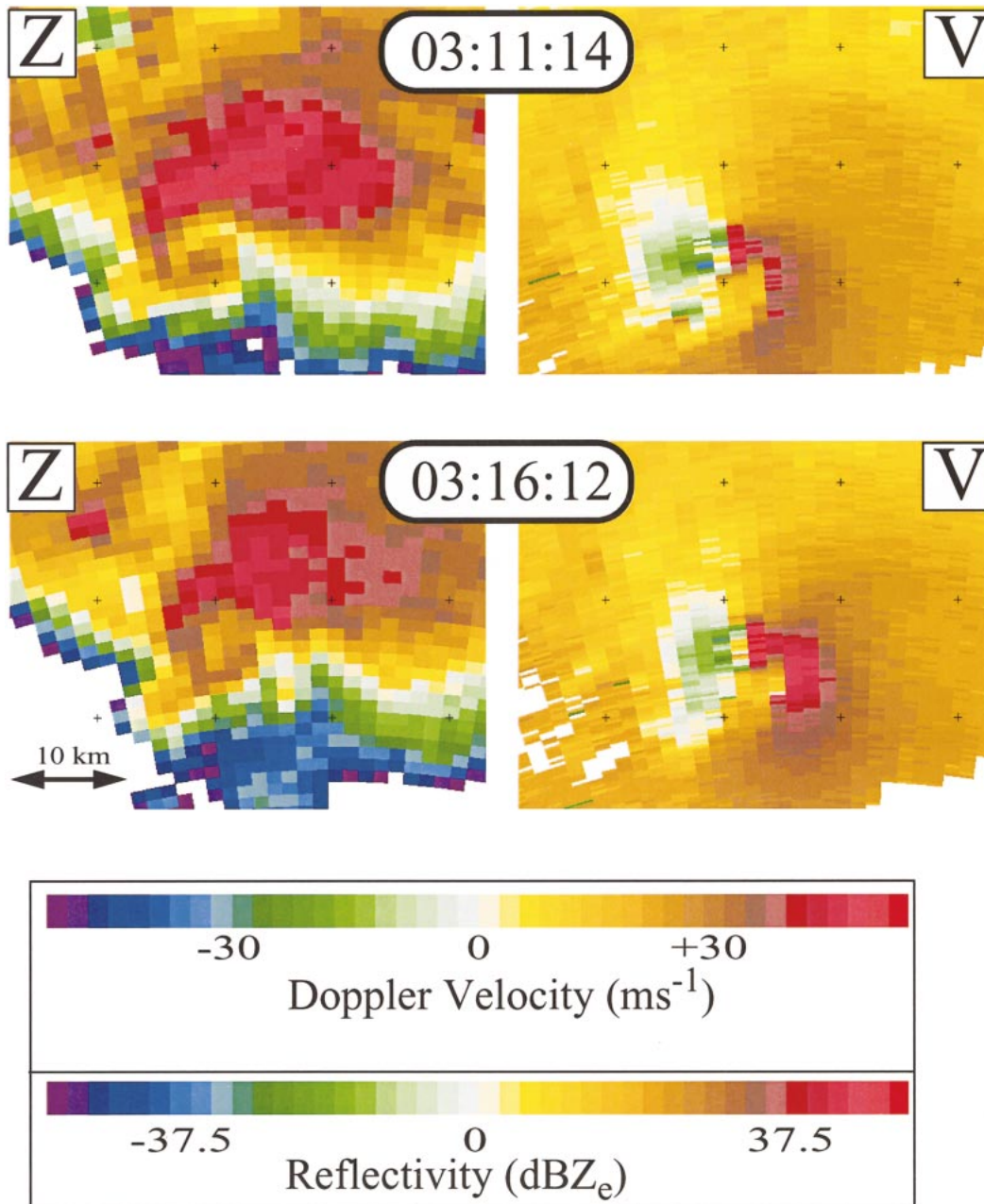
FIG. 3. (left) Reflectivity and (right) Doppler velocity fields at (top) 0311 UTC and (bottom) 0316 UTC 4 May 1999 as measured by the National Weather Service KTLX WSR-88D radar in the supercell thunderstorm that produced the tornado discussed herein. A very large and intense mesocyclone and large hook echo were persistent throughout the study period. Doppler velocity data have been subjectively dealiased. Tick marks are at 10-km intervals in this figure only.

the DOW resumed pursuit. These truly mobile observations were of lower quality and were difficult to locate precisely because of varying truck motion, location, orientation, and terrain blockage. See B for details. The three-dimensional azimuthally averaged structure and evolution of the horizontal and vertical wind fields, divergence, and pressure fields, including swirl-ratio calculations, as deduced from single-Doppler retrieval techniques, are presented in Lee and Wurman (2001, hereinafter LW). A detailed case study of the evolution and structure of this tornado during the entire observation period is in preparation for presentation elsewhere. The focus of this work is to document the multiple-vortex structure that was observed from 0310 to 0318 UTC, during the tornado's closest approach to the DOW.
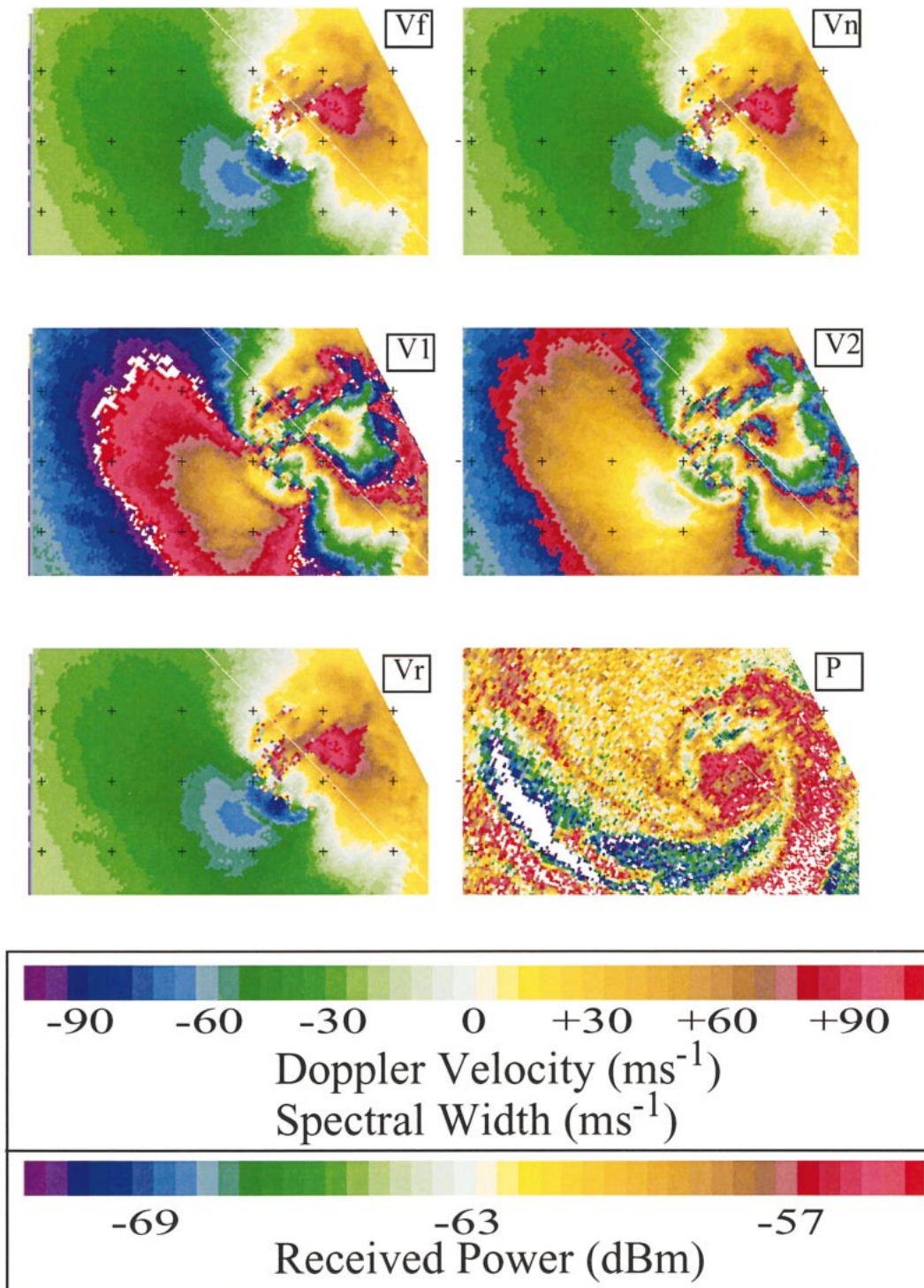
FIG. 4. Doppler velocity and received power (hereinafter ''power'') fields illustrating the staggered-PRT method and quality editing performed on the data used in all quantitative calculations presented herein and in some figures. (bottom left) Raw staggered-PRT velocity data Vr. (bottom right) Power in hook echo and debris cloud of tornado P. (center row) Raw, aliased, Doppler velocities calculated from each PRT in the staggered method, V1 and V2. (top right) Doppler velocity data Vn filtered objectively using NCP. (top left) Final Doppler velocities Vf after subjective editing for outlying values. The key in this figure applies to all remaining radar images and is not duplicated.
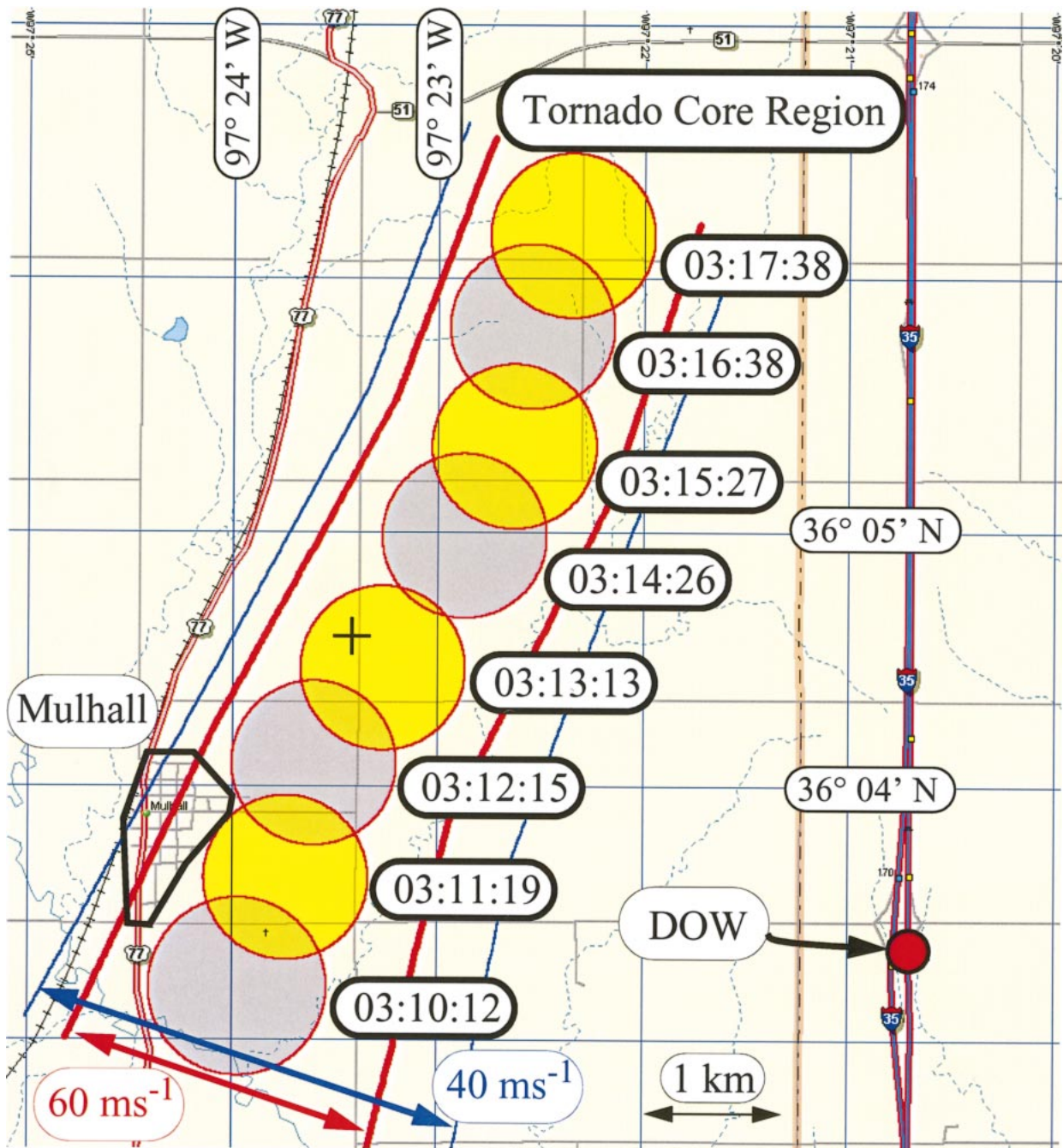
FIG. 5. Deployment location of DOW and tornado path. Location of the DOW (red circle) and the approximate diameter of the core flow and high-returned-power region, inferred to be the debris cloud, of the tornado each minute (circles) are shown. The town of Mulhall, OK, was impacted by the northwest edge of the tornado. The approximate extents of 60 and 40 m s^{-1} winds, as estimated from radar data, are delimited in red and blue lines, respectively.

c. Data collection strategy and data processing

Scanning was conducted through azimuthal sectors of approximately 85°, at 12 stepped elevation angles, crossing through the tornado between 30 and 1500 m AGL as shown in Table 1. The vertical spacing between the centers of the beams at the range of the tornado was 50–80 m below 400 m AGL and was 160–220 m from 400 to 1500 m AGL. Each scan required approximately 4–5 s to complete, resulting in volume scan intervals of approximately 60 s. Velocity and received power were processed using a staggered pulse repetition time (PRT) pulse-pair method, resulting in a Nyquist interval of 256 m s^{-1} (i.e., velocity aliasing occurred at ±128

FIG. 6. Visual image of part of the tornado at 0314:28 UTC taken from a video camera. The condensation funnel was partially illuminated by a lightning flash. The camera was pointing northwest. The northern edge of the condensation funnel was not captured in video images but was observable visually. The condensation funnel appeared, subjectively, to be over 1.6 km (1 mi) in diameter. The plotted time stamp is CDT (UTC − 5 h). (Courtesy of H. Stein.)

m s^{-1}), eliminating the need for subjective dealiasing of the velocities. Integration periods of 0.16 s (60 Hz) were chosen to provide an approximate factor-of-2 azimuthal oversampling to increase effective resolution (Wood and Brown 2000). Short pulse lengths (167 ns) were combined with two different rapid sampling intervals to produce 25- and 37.5-m nonoversampled range resolution during the observation period. The core flow region of the tornado approached to a range of approximately 3.5–4.5 km, resulting in a radar beam-

TABLE 1. Approximate elevation angles, tornado crossing altitudes, and interbeam spacing of radar beams in each volume scan.

Nominal elev angle of radar beam (°)	Approx alt of radar beam as it crossed tornado (m AGL)	Approx vertical spacing between scan and previous scan (m)
0	30	—
1	80	50
2	160	80
3	240	80
4	320	80
5	400	80
7	560	160
9	720	160
11	880	160
13	1100	~200
15	1300	~200
17	1500	~200

width of 65 m, with 32-m apparent resolution due to azimuthal oversampling. The resultant sample volumes of 25 m × 32 m × 32 m permitted scales of motion as small as about 100 m to be resolved well (Carbone et al. 1985). With a diameter of 1200–1700 m, the core flow region was resolved extremely well with about 50 samples in both azimuth and range directions, resulting in over 1500 samples per radar scan and 20 000 samples per radar volume. Data were processed and stored in a field format that could be translated into conventional radar quantities such as Doppler velocity (staggered PRT and each individual PRT), received power, equivalent radar reflectivity factor, normalized coherent power (staggered PRT and each individual PRT), and other derived quantities such as spectral width. Translation into NCAR Doppler Radar Data Exchange (DORADE) format, display, and editing were accomplished using the NCAR Solo software suite, routines Xltrs and Solo, with special scripts written to aid in sweep parsing. Data exhibiting normalized coherent power (NCP) values below 0.2 were filtered objectively. Occasional outlying velocity values probably caused by clutter, noise, or anomalously moving highly reflective debris were subjectively omitted from quantitative calculations and/or edited from figures. Data illustrating this process, and the velocities calculated using each individual PRT, staggered-PRT, and the objective and subjective filtering
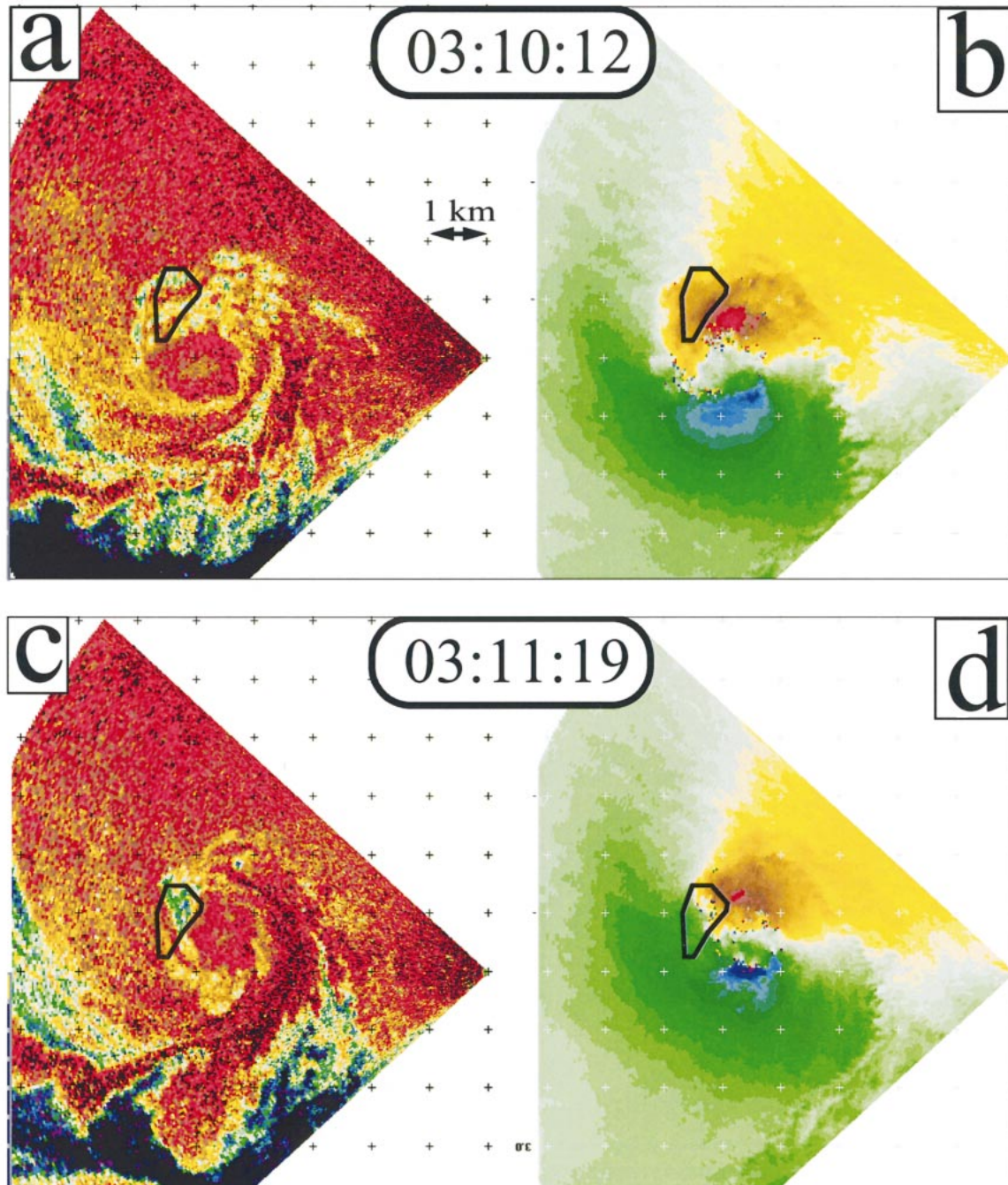
FIG. 7. (left) Power and (right) Doppler velocity fields in tornado in lowest repeatedly observable level, 70–160 m AGL, in each successive volume scan, spaced at approximately 60-s intervals. The debris cloud was visible in all images as a quasi-circular region of high power. This was connected to the tip of the hook echo, which was only partially visible because of the proximity of the DOW to the tornado. Precipitation wrapped completely around the hook echo and spiraled into the tornado from the northwest. The large tornadic circulation surrounding a more quiescent core flow region weakened gradually with time. Outside the region of maximum velocity, winds decreased gradually out to 3 km or more from the center of the circulation. Multiple wind field maxima, similar to those presented by Wurman et al. (1996a) were visible at several times. Intense subtornadic-scale vortices were evident, particular after 0313 UTC. They were manifested as local minima in power and as intense shear zones in velocity with length scales typically larger than the minimum resolvable scale of ~100 m.
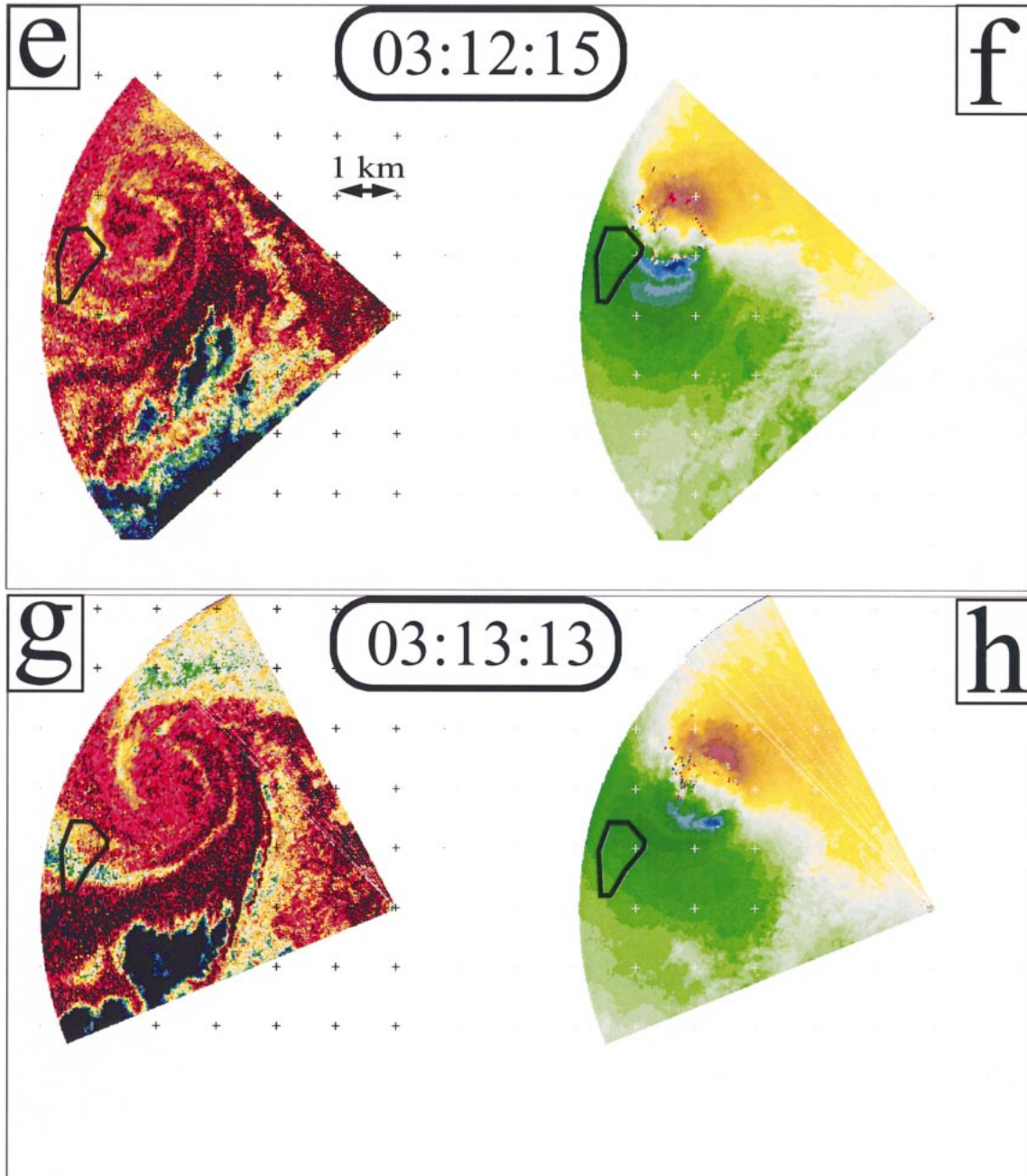
FIG. 7. (*Continued*)

are shown in Fig. 4. Velocity values produced using each individual PRT are used to calculate the staggered-PRT expanded Nyquist velocity field. Throughout this paper, received power (hereinafter ''power'') is used rather than equivalent radar reflectivity (dBZ_e). This is because the DOW system was not calibrated, because the data suffered from variable attenuation as the radar beams passed through the debris and rain fields of the tornado, and because the strong power returns from the tornado debris cloud sometimes saturated the receiving hardware, precluding accurate dBZ_e calculations. Doppler velocities were assumed to be representative of air parcel motions even though the dominant scatterers were likely small debris and rain. Because the tornado circulation was large, the differences between particle and air parcel motions due to particle transit through small regions of high air velocity (Dowell et al. 2001) were likely minimal. This may not have been true in the multiple vortices, in which particle trajectories may have resulted in very short residence times in regions
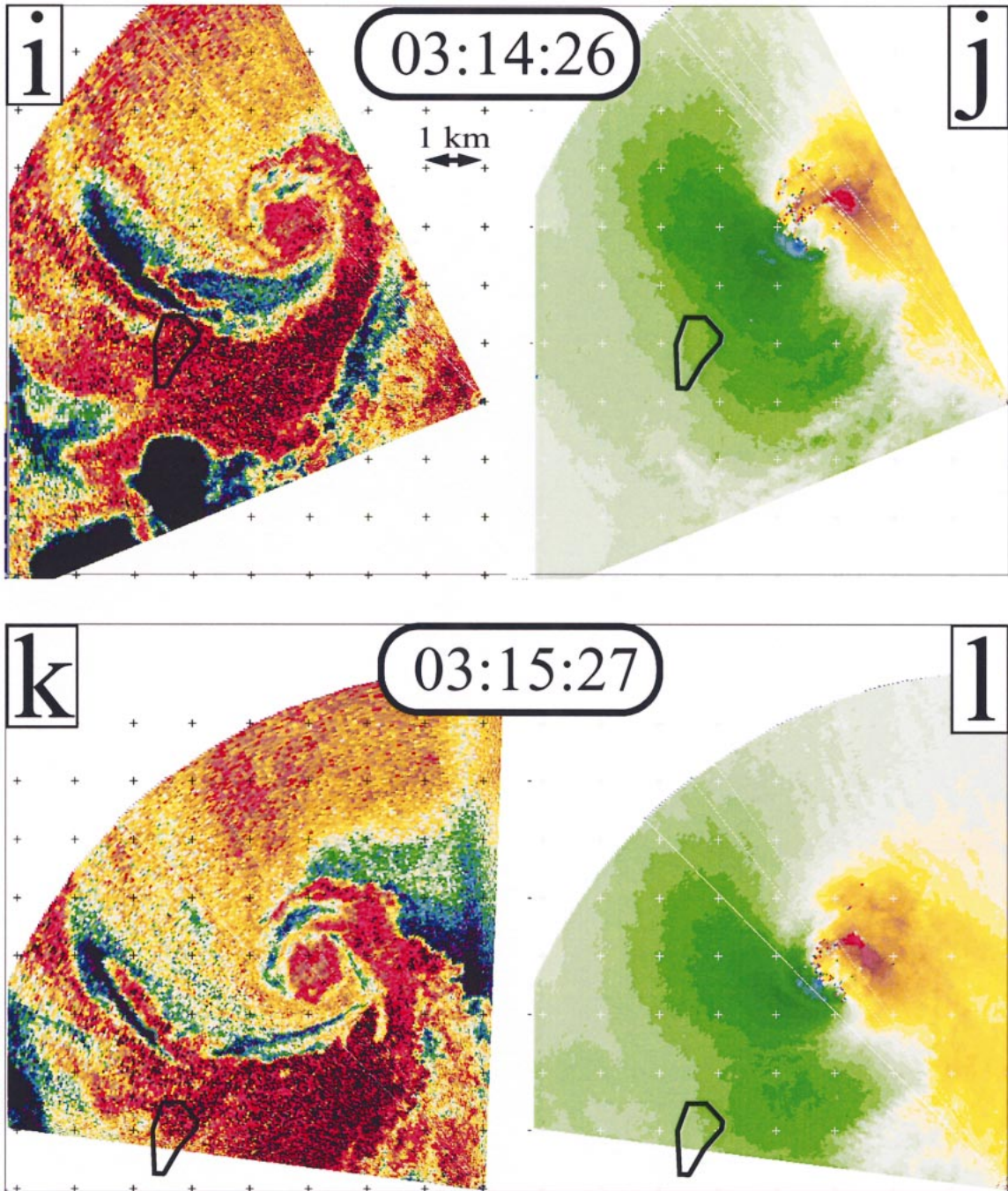
FIG. 7. (*Continued*)

with the most intense air velocities. Quantification of this complex effect, which would likely have resulted in the observations presented herein being *underestimates* of true multiple vortex intensity, is beyond the scope of this study.

The tornado was moving rapidly, at about 13.5 m s^{-1}, and was intercepted well after dark [2210–2228 central daylight time (CDT)]. This situation complicated site selection and deployment. Radar beams were partially blocked by terrain and trees below approximately 1.5° at various azimuthal angles. Furthermore, the condensation funnel and/or debris cloud of the tornado, when illuminated by lightning, appeared to be alarmingly large, with a diameter of as much as 1.5–2 km, and the real-time data from the DOW display revealed that dangerous winds extended well over a kilometer from the
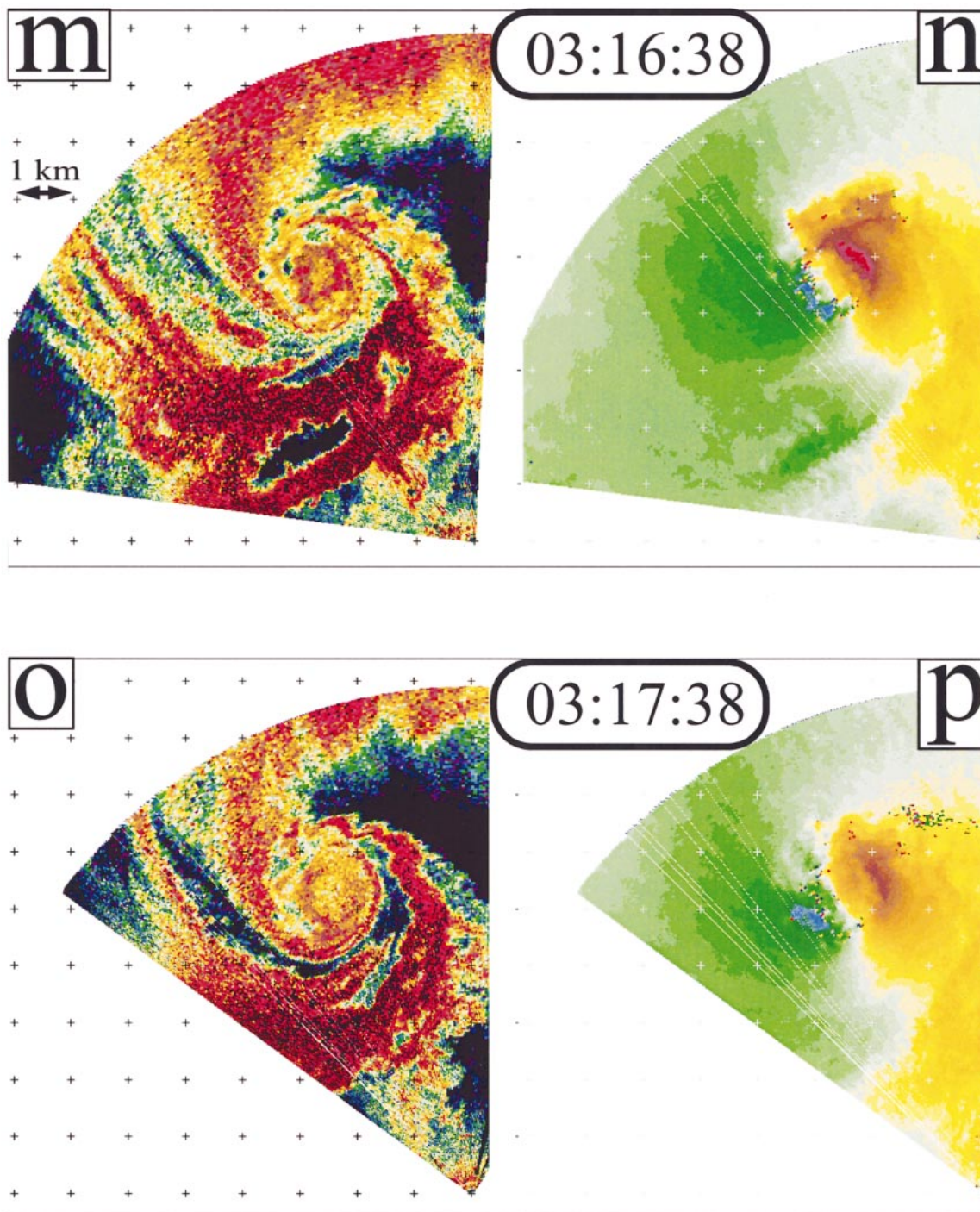
Fig. 7. (*Continued*)

center of rotation. For these reasons, a deployment site relatively far away (as compared with that chosen near the Spencer, South Dakota, tornado, for example) from the predicted track was chosen, precluding ultra high resolution observations. The approximate deployment location and tornado track are illustrated in Fig. 5.

3. Overview of the tornado

The tornado was exceptionally large and contained very high winds. Visual observations were difficult because it was well after sunset. However, some images were collected using a video camera when lightning
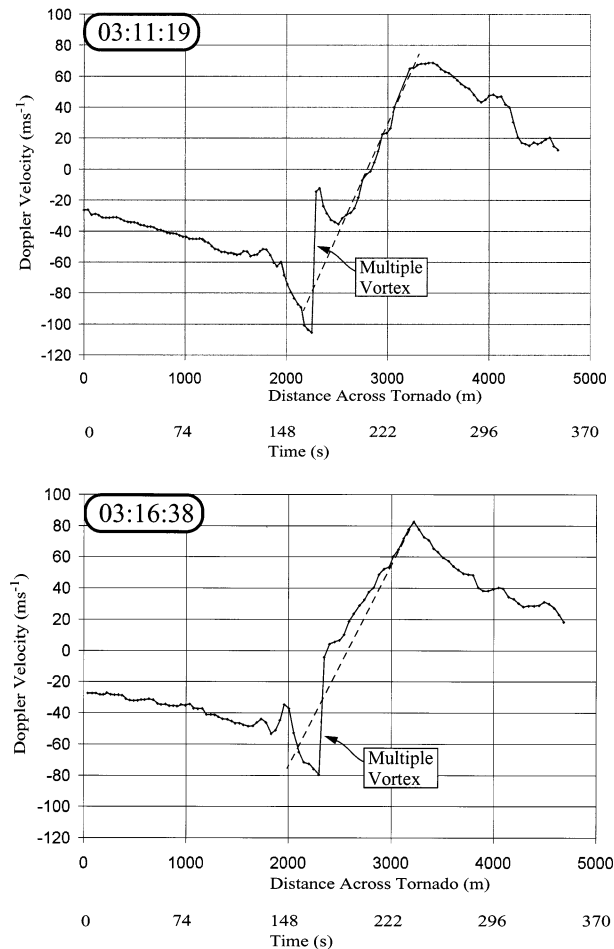
FIG. 8. Doppler velocity cross sections across the tornado at two times, early and late during the observation period. In both sections, the gradual decrease of winds outside the core radius of the tornado was evident. Nearly ideal solid-body rotation occurred in the core region, away from the multiple vortices. Significant velocity perturbations were observed in the vicinity of multiple vortices. Intense, gate-to-gate shear regions existed at the center of the multiple vortices where wind speeds changed by up to 100 m s^{-1} in as little as 50 m. A time–space conversion at 13.5 m s^{-1} was used to calculate the time-along-path axes.

illuminated the large, wedge-shaped condensation funnel (Fig. 6). During the study period, 0309:54–0318:05 UTC 4 May 1999, a large disk exhibiting high returned power, probably consisting of debris and rain as discussed below, centered at 4.2–5.7-km range, demarked the tornado (Fig. 7). The tornado moved in a generally north-northeasterly direction at 11–15 m s^{-1}, averaging 13.5 m s^{-1}. The center of the tornado passed just to the southeast of Mulhall, Oklahoma, causing several deaths and considerable damage, rated at F4 by National Weather Service damage surveys (Speheger et al. 2002). Based on DOW observations, it is estimated that parts of Mulhall experienced winds well in excess of 80 m s^{-1} (Figs. 5 and 7). The high power observed throughout the core flow region of the tornado was similar in appearance to that of the Spencer, South Dakota, tornado of 1998 that contained multiple vortices (Fig. 1) but contrasted sharply with the distinct low-power-eye visible tornadoes in which no multiple vortices were observed (WG; B; Wurman et al. 1996a). The highly reflective debris disk was generally about 1.2 km in diameter near the surface. The ring exhibiting the highest returned power had a diameter of 0.8–1.0 km.

The spatial scale of the low-level tornadic circulation of this tornado was the largest ever mapped by radar. The distance between the peak inbound and peak outbound velocities, denoting the diameter of the core flow of the vortex, was typically over 1.2 km near the ground and sometimes as large as 1.75 km several hundred meters AGL. Winds in excess of 50 m s^{-1} extended across a 2.5-km-diameter region. Winds in excess of 30 m s^{-1} extended across 4.5 km. The extremely large circulation contained Doppler velocities exceeding 100 m s^{-1} in places, with peak Doppler velocities in excess of 109 m s^{-1}. [All Doppler velocities reported in this paper were as measured by the radar and were not adjusted for tornado motion relative to the radar. Thus they did not exactly represent either tornado-center-relative tangential winds or ground-relative winds at any particular locations. Because the tornado was moving approximately tangentially to the radar during most of the study period (Fig. 5), the reported wind fields were a good representation of the tornado-relative wind fields on the north-northwest and south-southeast sides of the tornado. For a discussion of wind field adjustments that account for these and other factors, see WG.] Doppler velocities in two cross sections through the tornado are illustrated in Fig. 8. The large core flow region of the tornado, exhibiting approximately solid-body rotation with an average shear of [160 m s^{-1} (1200 m)$^{-1}$] = 0.13 s^{-1}, and the outer velocity decay region are evident in both cross sections. The velocities V outside of the core flow region decay with an approximately $V \propto R^{-0.5}$– $V \propto R^{-0.6}$ dependence, as observed by the DOWs in other tornadoes (WG). However, the decay rate was sometimes closer to $V \propto R^{-1}$ as predicted by frequently used conceptual models (Zrnić and Doviak 1975; Burgess et al. 1993; Bluestein et al. 1993; Wood and Brown 1997; Burgers 1948; Rott 1959). Generally, lower values of estimated circulation, $C = 2\pi VR$ (not plotted), were evident near the radius of peak tangential wind speeds, consistent with the frictional losses observed in WG, but the value is nearly constant on one side of the tornado in one of the cross sections, consistent with flow models predicting $V \propto R^{-1}$. Plotted profiles were chosen to illustrate the perturbations to the primary tornadic circulation associated with two multiple vortices.

It is likely, based on the extremely high winds observed over 1 km from the center of circulation, that the almost-circular band of high returned power surrounding the central reflective disk was also composed of dust and debris in addition to rain. This would be consistent with previous DOW observations in which

TABLE 2. Comparative sizes of various large tornadoes measured by the DOW radars. The Mulhall tornado studies herein was by far the largest. Maximum observed Doppler velocity (V_{max}) values were obtained using different resolution volumes and were not corrected for tornado motion or other effects (WG), so they may not be exactly comparable, but they serve to illustrate this qualitative comparison. The diameter of the core flow region is D_{core}, and Diam ($1/2V_{max}$) is the diameter of the region containing winds of at least $0.5V_{max}$.

Tornado	V_{max} (m)	D_{core} (m)	Diam ($1/2V_{max}$) (m)
Dimmitt	74	200	800
Spencer	100	300	1200
Oklahoma City	130	400	800
Mulhall	109	1200	3000

the debris cloud of a tornado was roughly coincident with the region containing winds greater than 30–40 m s^{-1}. Describing the "size" of any tornado is problematic because there are no standard definitions. Tornadoes measured by the DOWs or other high-resolution radars can be characterized based on the diameters of the core flows. However, if the intensity of the peak winds is very high, substantial amounts of lofted debris may exist outside of this region, causing disparity between this and visually indicated sizes. Furthermore, the diameter of the condensation funnel of a tornado may be less than or greater than the diameter of the core flow region depending on the tornado intensity and the environmental humidity. Intense tornadoes are capable of producing damage well away from the radius of peak winds, and weak tornadoes may cause only intermittent or undetectable damage, so damage swath widths may be very different from the diameter of the core flow region and may be modulated significantly by the presence and locations of multiple vortices. In the case of the tornado studied herein, the winds at the outer edge of the central debris ring (diameter 1.2 km and indicated in later figures detailing subtornado-scale structures) were often in excess of 80 m s^{-1}, so the edge of this ring was well within the region of the potentially damaging tornadic winds. The absence of high power over the region impacted by 50–80 m s^{-1} winds suggested that strong inflow, with little or no upward component, carried debris toward the core flow region at or below the lowest repeatedly observed level of about 70 m. This was consistent with three-dimensional single-Doppler wind field retrievals in this tornado (LW). One working definition of the size of a strong tornado is the region containing winds at least as strong as some (unfortunately arbitrary) fraction of the peak velocity. The region that contained winds of at least one-half of the typical azimuthally averaged peak tornado velocity (80 m s^{-1} × 0.5 = 40 m s^{-1}) was approximately a circle with a diameter of 3 km, enclosing 7 km^2. By contrast, using the same definition, the diameters of the strong Dimmitt, Texas (2 June 1995), and the Bridge Creek–Moore–Oklahoma City (3 May 1999) tornadoes using a similar definition were only about 800 m, enclosing 0.5 km^2, and the

diameter of the Spencer, South Dakota, tornado (30 May 1998) was about 1.2 km, enclosing 1.1 km^2. By almost any measure (Table 2), the tornado studied here was significantly larger than most.

4. Multiple-vortex structure

a. Overview of the multiple-vortex structure

A pronounced multiple-vortex structure was often evident in the Doppler velocity, power, and spectral-width data. Although the range of the tornado to the DOW would not have permitted the observation of small-scale (10 m) multiple vortices, this tornado contained multiple vortices of a much greater size. The vortices revolved around the center of the primary circulation and were tracked from sweep to subsequent sweep as the radar beam crossed through the tornado every 4–5 s. The primary tornadic circulation was significantly modulated by the rotating multiple vortices, so much so that the Doppler velocity occasionally reversed in the region of the multiple vortices. Figure 7 illustrates the Doppler wind field of the core flow region of the tornado at approximately 100 m AGL (70–160 m AGL) at approximately 60-s intervals. The scale of the primary circulation contracted so that the core diameter decreased from approximately 1600 m at 0310:12 UTC to 1200–1300 m through 0317:38 UTC. More important, the velocity signature of several multiple vortices were present at various locations in the various slices, in particular after 0312 UTC, as the tornado weakened and contracted slightly, likely affecting the swirl ratio (Davies-Jones 1976). Swirl ratio calculations have been made in a separate study (LW), but uncertainties in the calculations preclude the discerning of a definitive increase in the swirl ratio during the observational period.

The velocity differences ΔV across these vortices sometimes exceeded 100 m s^{-1} (peaking at over 120 m s^{-1}) over distances sometimes less than 100 m, but more typically 200–300 m, representing approximately 50% of the total azimuthal shear present in the tornado. Peak Doppler velocities in the vortices were as high as 109.5 m s^{-1}, about 1.2–1.5 times the estimated peak azimuthally averaged tangential velocities (V_{atp}; LW), well below the largest predicted to exist by some (Fiedler 1998; Fiedler and Rotunno 1986; Fujita 1970) but more consistent with the predictions of Lewellen et al. (1997). This comparison is imprecise because the radar observed only one component of the wind vector, so observed Doppler velocities were actually lower bounds on true wind speeds. Furthermore, Dowell et al. (2001) illustrate how Doppler velocities may underestimate true air motions in small tornadoes (and presumably, small multiple vortices) because of the short residence time of scattering particles in the peak airspeed regions. However, Doppler velocity differences of about 80–100 m s^{-1} across the multiple vortices implied approximately ±40–50 m s^{-1} perturbations to the background flow,
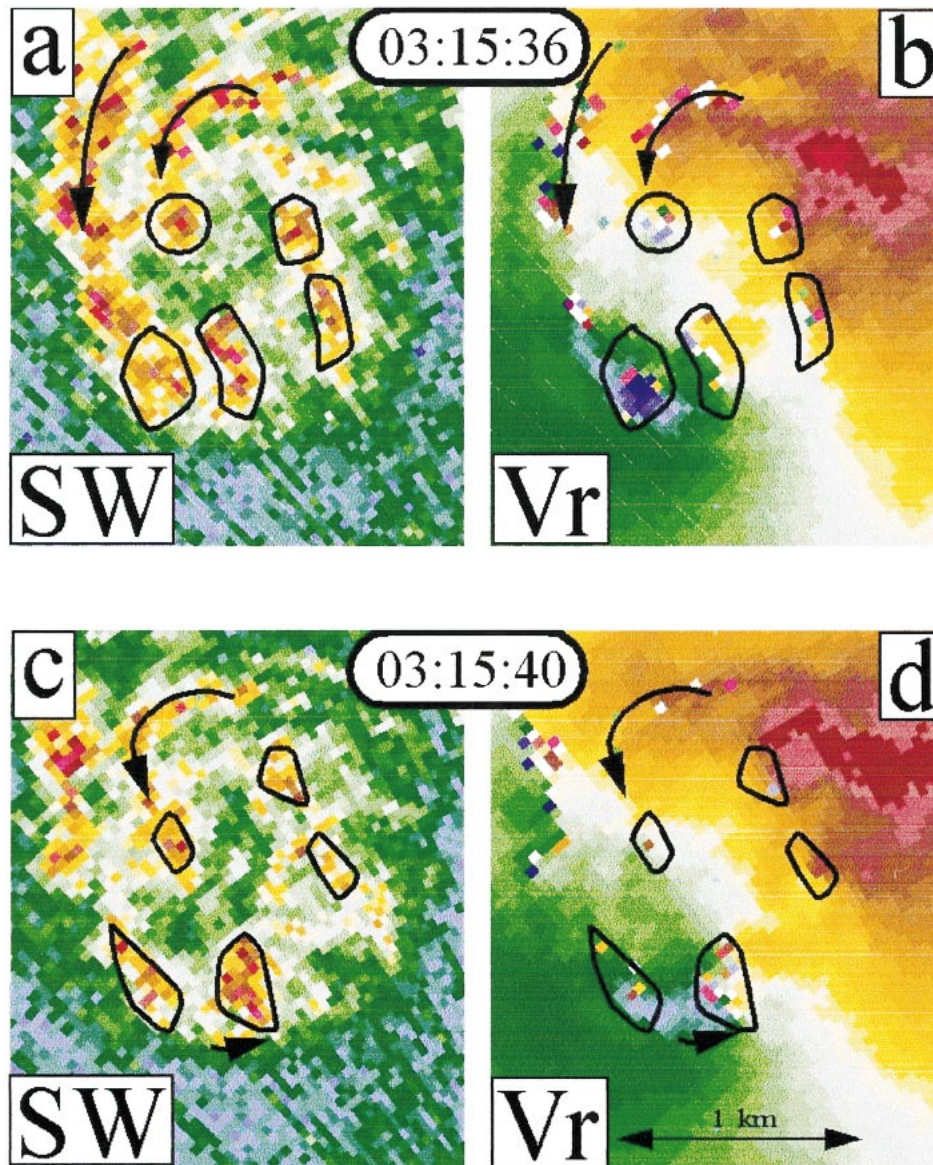
FIG. 9. Spectral width structure of tornado and multiple vortices. (a), (c), (e), Spectral width fields were compared with (b), (d), (f) Doppler velocity fields in selected scans through tornado. Regions of high spectral width, enclosed in black or indicated with black lines or arrows, were used in conjunction with power and velocity data to identify and to track individual vortices. When multiple vortices were not evident, or were weaker or smaller, the spectral width pattern and wind fields were more axially symmetric [(e) and (f)] with high values of spectral width surrounding a much less turbulent core at the center of the tornado. At other times, the spectral width field exhibited (g) spiral features or (h) other complex morphology.

considerably stronger than were observed in the Spencer tornado [Fig. 1 and Wurman (1999)]. Perturbations of 40–50 m s^{-1} added to the 70–80 m s^{-1} V_{atp} calculated in LW would result in peak wind speeds of 110–130 m s^{-1}, or about 1.5V_{atp}. However, 109.5 m s^{-1} was the highest observed value, possibly because of the non-optimal location of multiple vortices during the brief moments of observation or because the peak additive multiple-vortex perturbation was outside the radius of V_{atp}. (The perturbations due to the multiple vortices were

not superimposed on a constant background velocity field, but rather on one that varied strongly with radius from the center of the tornado.) It is possible that much higher wind speeds occurred on scales not resolvable by the DOW. Peak shear values were 2–4 s^{-1}, with implied extreme vertical vorticities of 4–8 s^{-1}, by far the largest ever measured by radar in tornadic flows.

The typical horizontal scale of the multiple vortices, defined as the distance between the maximum positive and negative perturbations to the underlying tornado-
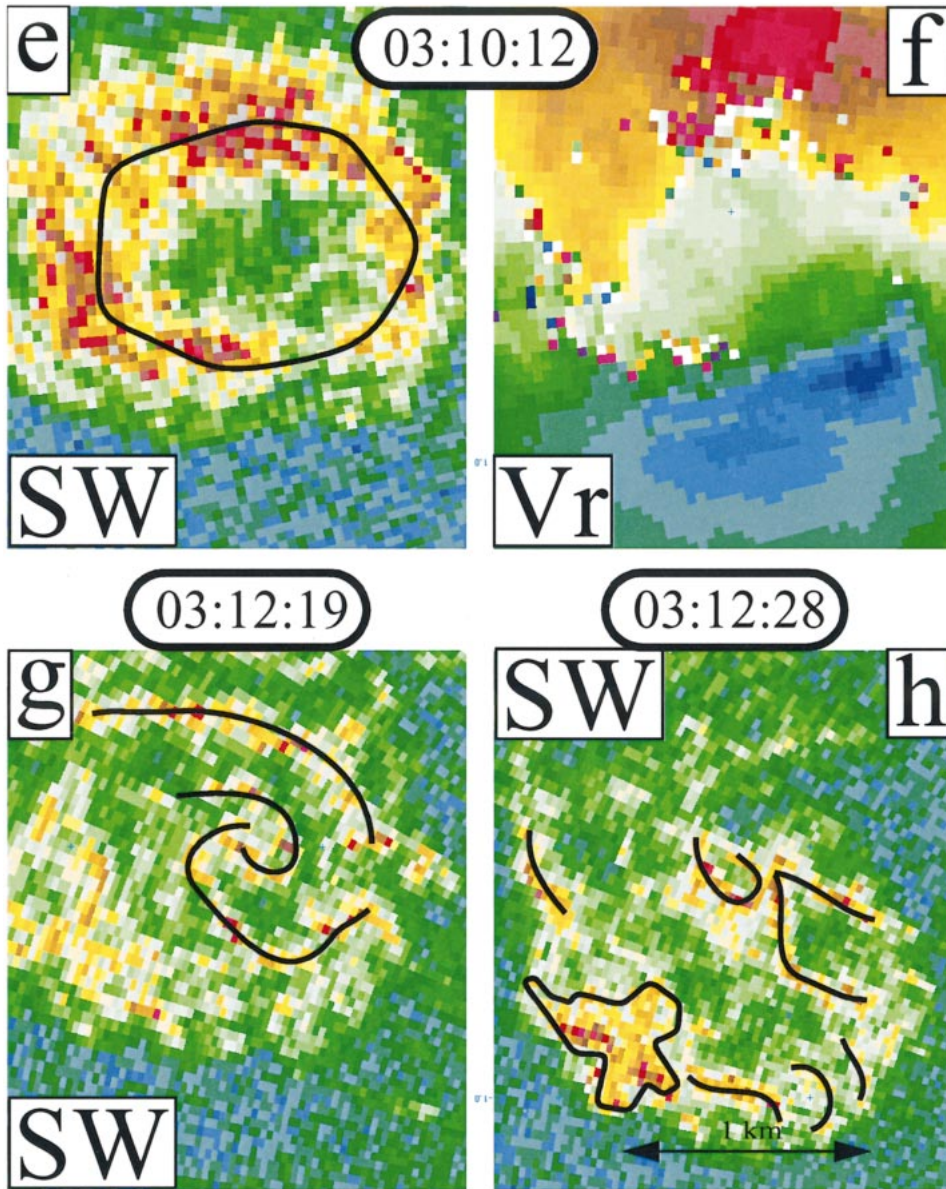
FIG. 9. (*Continued*)

scale flow, ranged from 100 to 500 m, with most exhibiting 200–300-m diameters. Much of the shear in the multiple vortices was concentrated in regions of 40–100 m or less (gate-to-gate shear observations), however, indicating a wind field structure very different from the approximately solid-body rotation observed in the core flow of this tornado (Fig. 8) or other tornadic circulations (WG; Wurman et al. 1996a).

The amplitude of the vortices decreased with altitude, and the size increased. The vortices propagated upstream in the parent tornadic flow at approximately 0.5–0.9 of the peak speed of the parent tornado, consistent with laboratory (Ward 1972) and numerical modeling studies (Rotunno 1984; Lewellen et al. 1997). However, because these models, and others (Walko and Gall 1984), predict backstream helical tilts to these vortices, it cannot be ruled out that the vortices were propagating at the speed of the background tornadic flow, consistent with Walko and Gall (1984). It was difficult to determine the background tornadic flow at the location of the vortices, so, because the vortices occurred near the radius of maximum background winds, the peak azimuthally averaged tangential values V_{atp}, were used as the standard for comparison with the background flow.

Although smaller vortices may have been present but unobservable by the DOW, it is believed, based on spec-
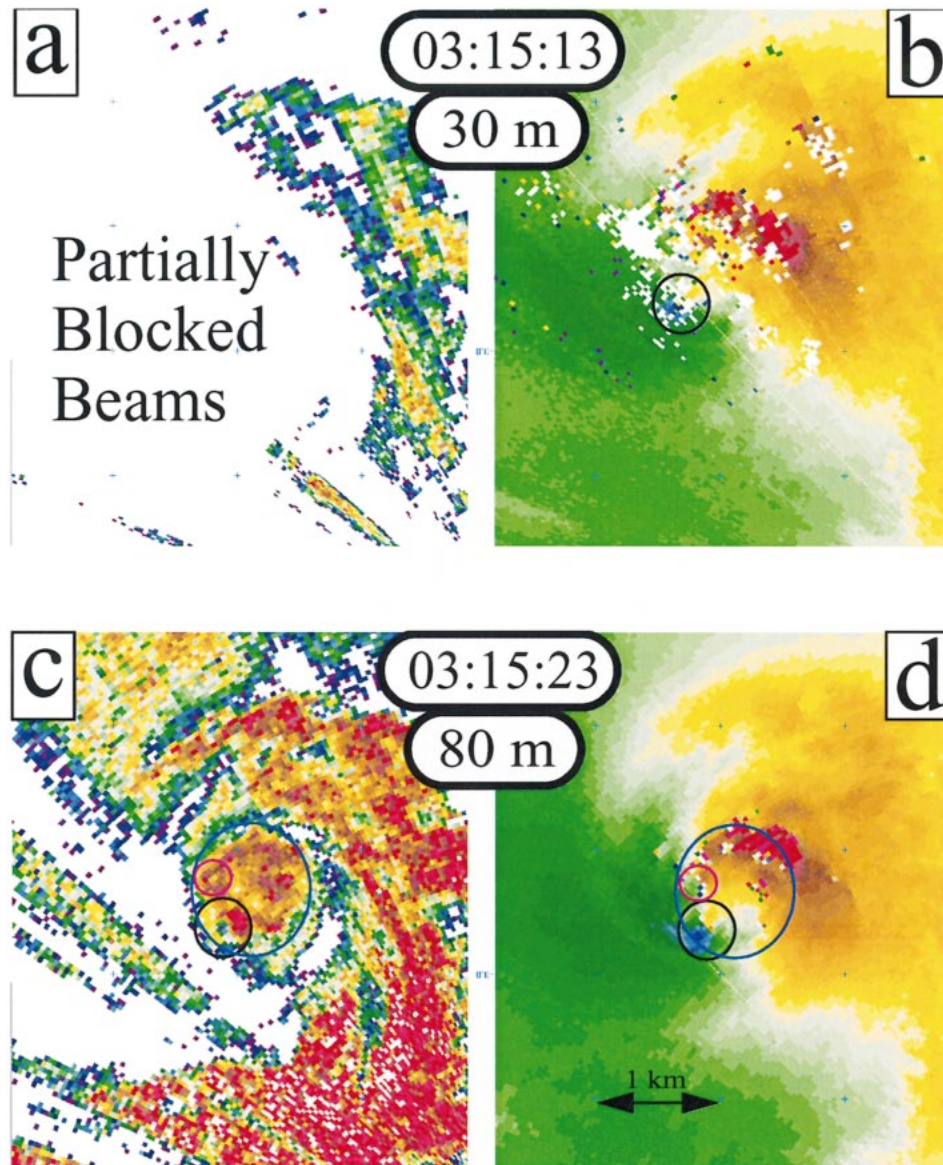
FIG. 10. Tracking of multiple vortices A and B. (left) Power and (right) Doppler velocity fields are shown in several subsequent scans through the tornado during a 1-min period. The approximate outline of the debris cloud (a surrogate for the region with upward vertical motion) is indicated with large dark blue ellipses except above 600 m AGL where it is less distinct. Multiple vortices A, B, and B′ are indicated by black (vortex A), pink (vortex B), and green (vortex B′) ellipses. Other possible vortices are indicated with yellow ellipses, but these were not tracked. The vortices, revolving about the center of the tornado, were manifested as high-power circles surrounding comparatively lower power eyes and by regions of intense wind shear and spectral width, which had spatial and temporal continuity. Plotted times represent the start times of the scans, not the times that scans passed through particular vortices. Plotted altitudes represent nominal heights AGL of each scan as it passed through the tornado.

tral-width evidence, discussed below, that the observed 200–300-m scale vortices dominated the nonaxisymmetric flow.

The multiple-vortex structure was clearly visible in the received power structure of the tornado. While tornadoes with less pronounced multiple vortices or those absent multiple vortices have exhibited distinct single low-reflectivity eyes (WG; Wurman et al. 1996a), the power signature of multiple-vortex tornadoes has been observed to be more complex, sometimes not containing central eyes (see Fig. 1 and Wurman 1999). As will be seen below, multiple low-power eyes were unambiguously associated with individual vortices. Some of the vortices existed at the outer edge of the central disk and were associated with miniature hooklike returned power structures rather than enclosed eyes. Some existed just
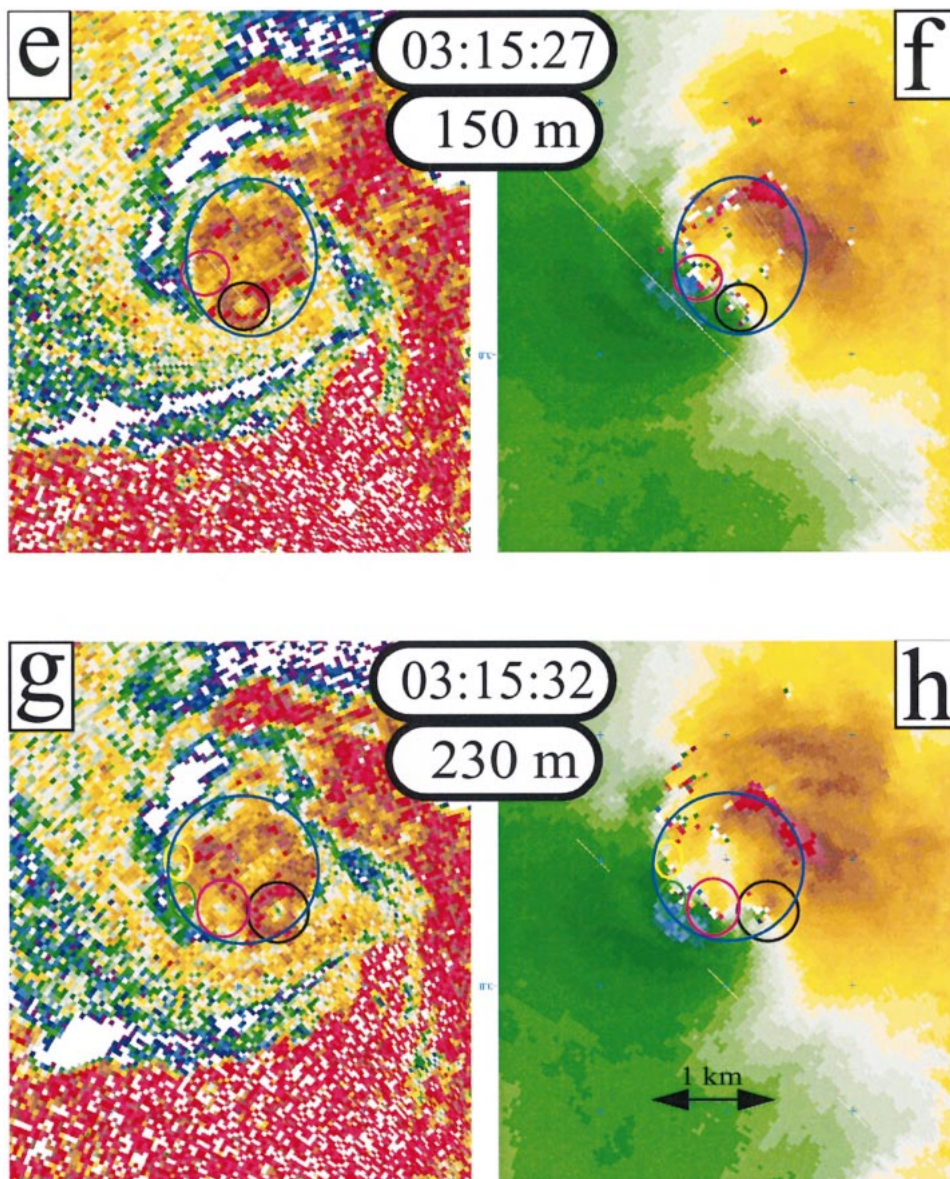
FIG. 10. (*Continued*)

inside the high-power region, suggesting that they were in the corner flow region where inwardly moving air was turning upward (Davies-Jones 1976; WG; LW), which is somewhat inconsistent with the numerical simulations of Lewellen et al. (1997) whose multiple vortices appeared ''well inside the core of maximum swirl velocity; they are centered between the annular updraft and the central downdraft within the tornado.'' However, because the vortices themselves perturbed the tornado flow and the boundary of the debris cloud significantly, it might be that they were actually inside the mean annular updraft. Furthermore, a few vortices, including vortex D, discussed below, did occur well within the debris cloud.

Spectral-width calculations also revealed the multiple-vortex structure of the tornado. Although the spectral-width fields were more difficult to interpret, regions of high and low spectral width, indicative of high and low turbulence and/or wind shear, were used to aid in the identification and tracking of individual vortices. Figure 9 illustrates the spectral-width field at selected times. High-spectral-width regions demark the centers of the multiple vortices (Figs. 9a–d,g,h, black ovals) and intense shear zones where winds appeared to be spiraling in toward these vortices (Figs. 9a–d, g,h, black curved lines). When multiple vortices were less prominent (Fig. 9e,f), rings of high spectral width surrounded regions of very low spectral widths, just 2–3 m s^{-1},
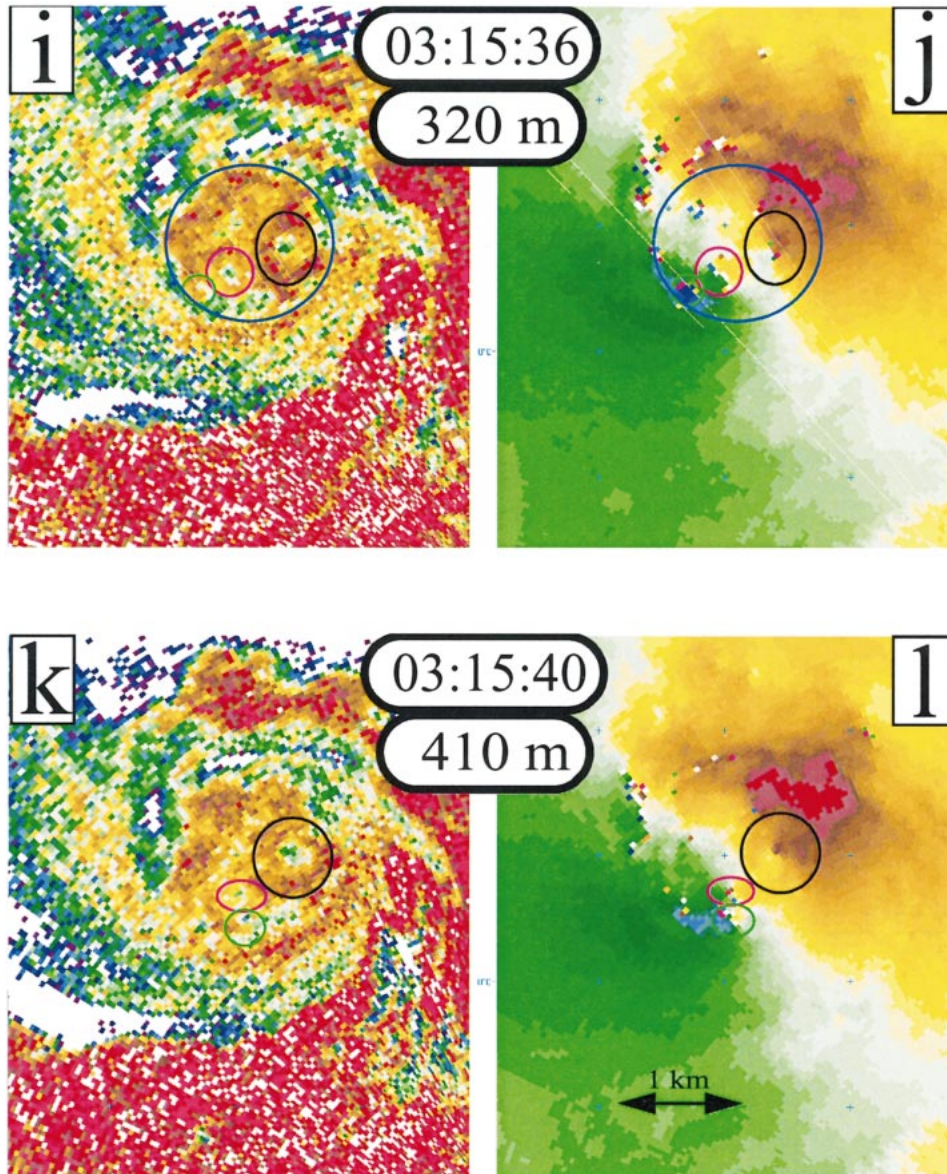
FIG. 10. (*Continued*)

near the center of the tornado, implying that the latter regions were regions of low turbulence. At other times, the spectral-width fields appeared to be very complex and were difficult to interpret (Fig. 9h).

There are isolated gates of high spectral width in certain radar scans. These can be seen in Figs. 9a and 9g. These may be indicative of multiple vortices with scales of less than 100 m that were not fully resolvable in this study. However, the spectral-width values in these smaller regions are lower than those in the larger regions more clearly associated with multiple vortices. This observation and the apparent paucity of multiple vortices with scales near the minimum observational scale suggest that the observed preferred scale of about 200–300

m was indeed the true preferred scale. This is also consistent with models (Walko and Gall 1984) that showed that the most rapidly growing unstable modes varied from about wavenumber 2 to wavenumber 5 over a broad range of swirl ratios. The comparison of the "scale" values presented herein with wavenumbers is not direct. This is because the spacing of the observed multiple vortices is usually 2–4 times the distance between the maximum perturbation velocities. Therefore, the observed vortices in this tornado exhibit wavenumbers of approximately $(1300 \text{ m})\pi/(3 \times 250 \text{ m})$, or about 6. Vortices in this large tornado with horizontal scales of less than 100 m would exhibit wavenumbers of greater than 10. Closely spaced smaller multiple vor-
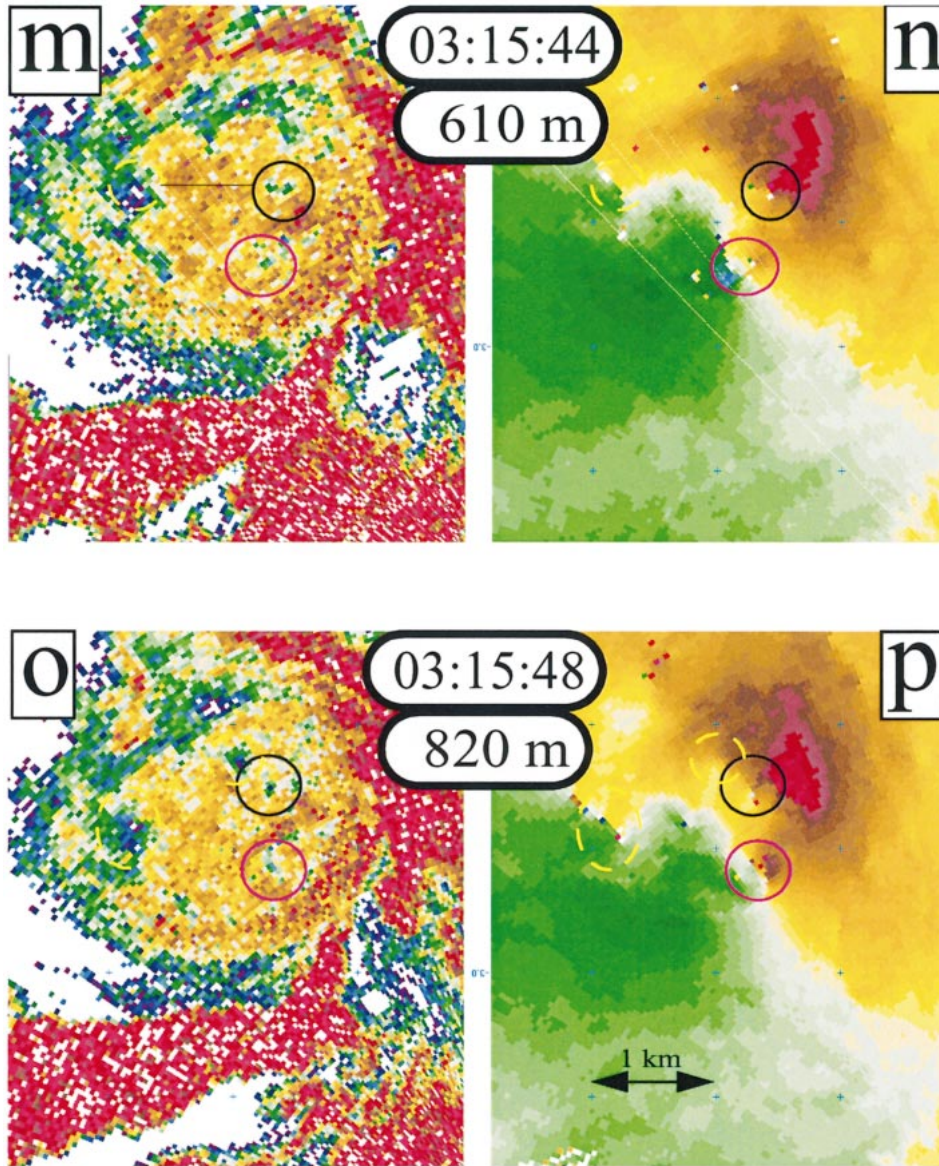
FIG. 10. (*Continued*)

tices, possibly with wavenumbers as high as 10, were observed during the end of the study period after 0316 UTC and are discussed in section 4f.

b. Tracking individual vortices

The DOW completed horizontal scans through the tornado at roughly 4–5-s intervals. The elevation of the beams at the range of the tornado proceeded in approximately the manner described above, though the exact altitude varied with each scan and with location within the tornado. By making the assumptions that the inclination of the multiple vortices did not change appreciably in the 4–5 s required for the beam to revisit a region of the tornado and that the axes of rotation of the vortices were not tilted nearly horizontally, it was possible to neglect the fact that successive scans were occurring at increasing altitude and to track the horizontal movement of the vortices. The vortices translated approximately 250 m between sweeps, much more than the elevation difference between adjacent observations, particularly below 400 m AGL. Spurious apparent motion would have been introduced by any helical tilting of the vortices upwind, consistent with numerical simulations (Rotunno 1984; Walko and Gall 1984; Lewellen et al. 1997). If the angle of tilt was very large, say 45°, it would have introduced an error of about 50–80 m in the lowest 400 m AGL, introducing a false retrograde motion of only 25%–35% of the calculated translational velocity. For that reason the calculated translational
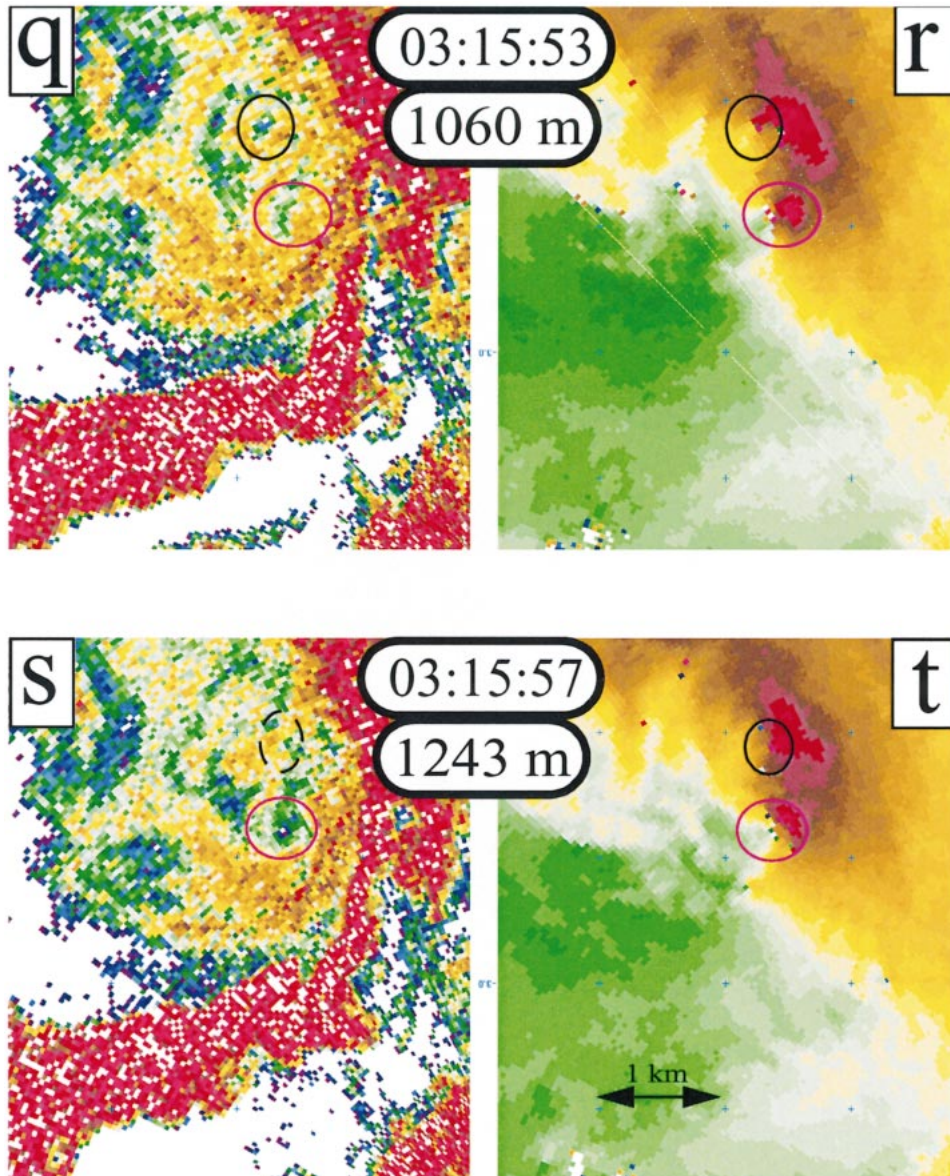
FIG. 10. (*Continued*)

speeds presented herein are likely to be close to, but somewhat lower than, the actual values. Because the vortices were typically trackable through about 180° of rotation about the parent tornado, the superposition of the tornado translational speed relative to the ground (about 13.5 m s⁻¹) to the multiple vortex translational speed about the tornado was neglected, and average translational speeds are reported herein. Because this tornado was translating and the computational and laboratory studies with which these data were compared simulated stationary tornadoes, these comparisons were only approximate in any case. The vertical structure of the vortices was deduced from slices taken at slightly different times, so temporal evolution—strengthening,

weakening, contraction or expansion, or change of morphology—would contaminate these calculations. Because the behavior of the several different multiple vortices discussed below was similar in many ways, however, the described structure and behavior are probably representative.

The multiple-vortex pattern in this tornado was very complex. It is likely that some vortices were transient and/or interacted in complex fashions with other vortices. Nevertheless, the extremely large nature of the parent tornado, the correspondingly large size of the vortices, and the relatively rapid scanning of the DOW combined to allow the tracking of several persistent circulations, which are discussed below.
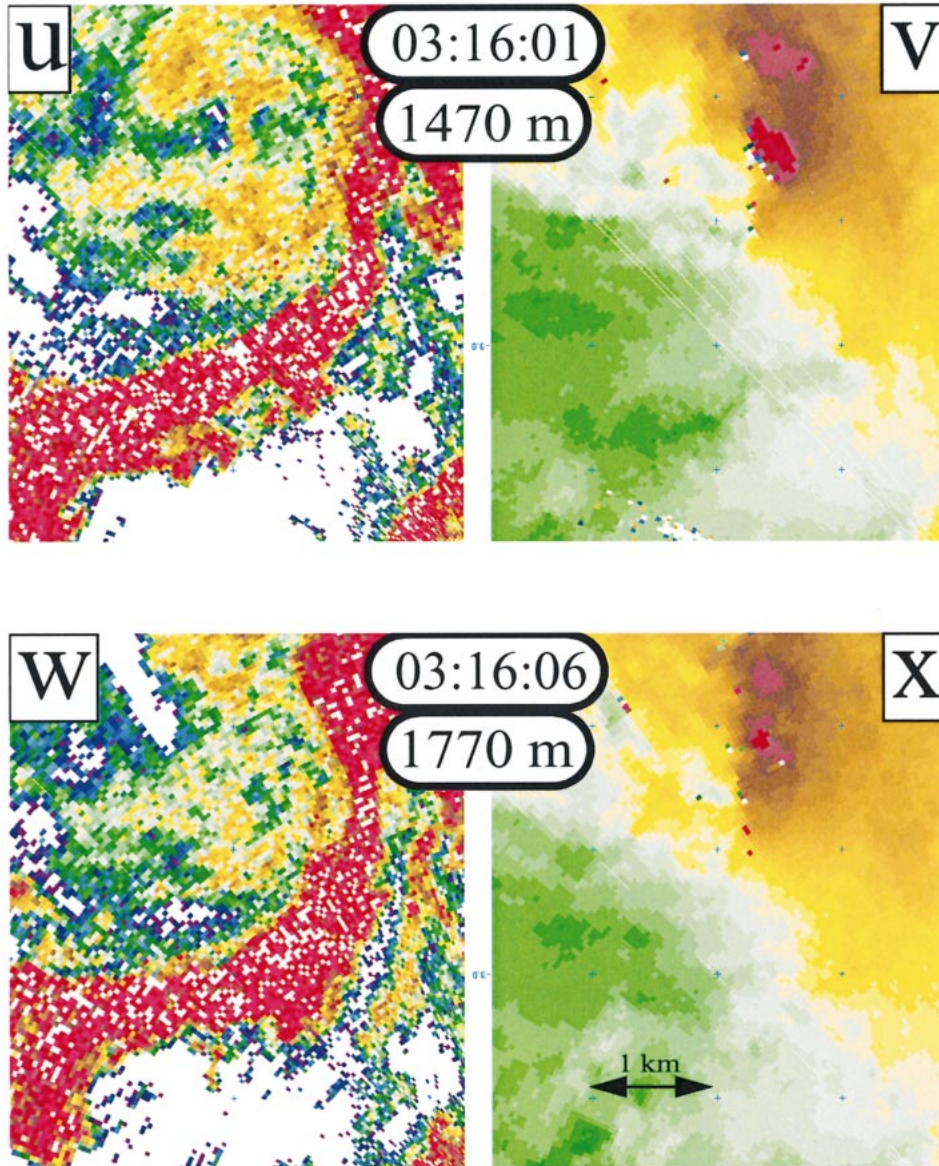
FIG. 10. (*Continued*)

c. Vortex A

Vortex A was tracked for over 40 s as it rotated around the tornado, through about 240°. The Doppler velocity and power fields in this vortex at several different times and altitudes from one radar volume scan are presented in Fig. 10. Vortex A was first observed very near the surface on the southwestern side of the tornado at 0315:21.3 UTC (Fig. 10b). This vortex is highlighted throughout Fig. 10 with a black oval. Note that the altitudes plotted in figures are the nominal altitude AGL at which the beam crossed the tornado. The actual altitude at which the beam crossed this and other multiple vortices varied by a few meters from this value because of antenna pointing variations and beam inclination.

These differences were less than the radar beamwidth of about 75 m. The plotted times represent the start times of each scan, not the times that the scans crossed any particular vortices.

This vortex exhibited a distinct and trackable doughnut-with-hole-type power signature (Figs. 10 c, e, g, i, k, m, o, q) with some characteristics similar to that of a single-cell vortex tornado (WG; B). Beam blockage prevented satisfactory power data from being collected at the lowest scanned level, but, above that, the vortex was characterized by a low-power eye surrounded by a ring of higher values. The diameter of the ring (from peak value to peak value) was approximately 200–300 m at the lowest levels. This was consistent
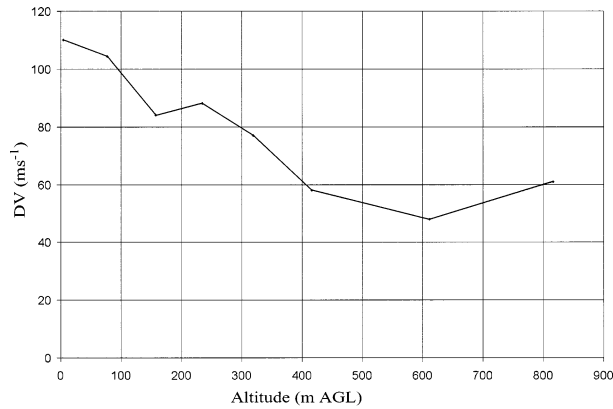
FIG. 11. Doppler velocity difference ΔV across vortex A as a function of altitude. The ΔV was more than 100 m s^{-1} near the ground and decreased to about one-half of that value above 500 m AGL.

with the size of the vortex inferred from the distance between the peak inbound and peak outbound radial velocities (discussed below). The diameter of the high-power ring increased with altitude until it was 400 m in diameter at 415 m AGL. During the 21.6 s between the observations at 78 m AGL (0315:25.8 UTC) and 611 m AGL (0315:47.4 UTC), the vortex had revolved from the southwest, through the south, east, then north side of the parent tornado. Above 611 m AGL, the power signature was difficult to track and appeared to become split, exhibiting a double eye.

The difference in Doppler velocity ΔV across the vortex was in excess of 100 m s^{-1} at the lowest observed levels but decreased substantially with height (Figs. 10 b, d, f, h, j, l, n, p, r, t and 11). The ΔV across the vortex was over 50% of the ΔV across the entire tornado at the lowest levels but was proportionately less aloft. Vertical vorticity ζ was approximated by the formula $\zeta =$
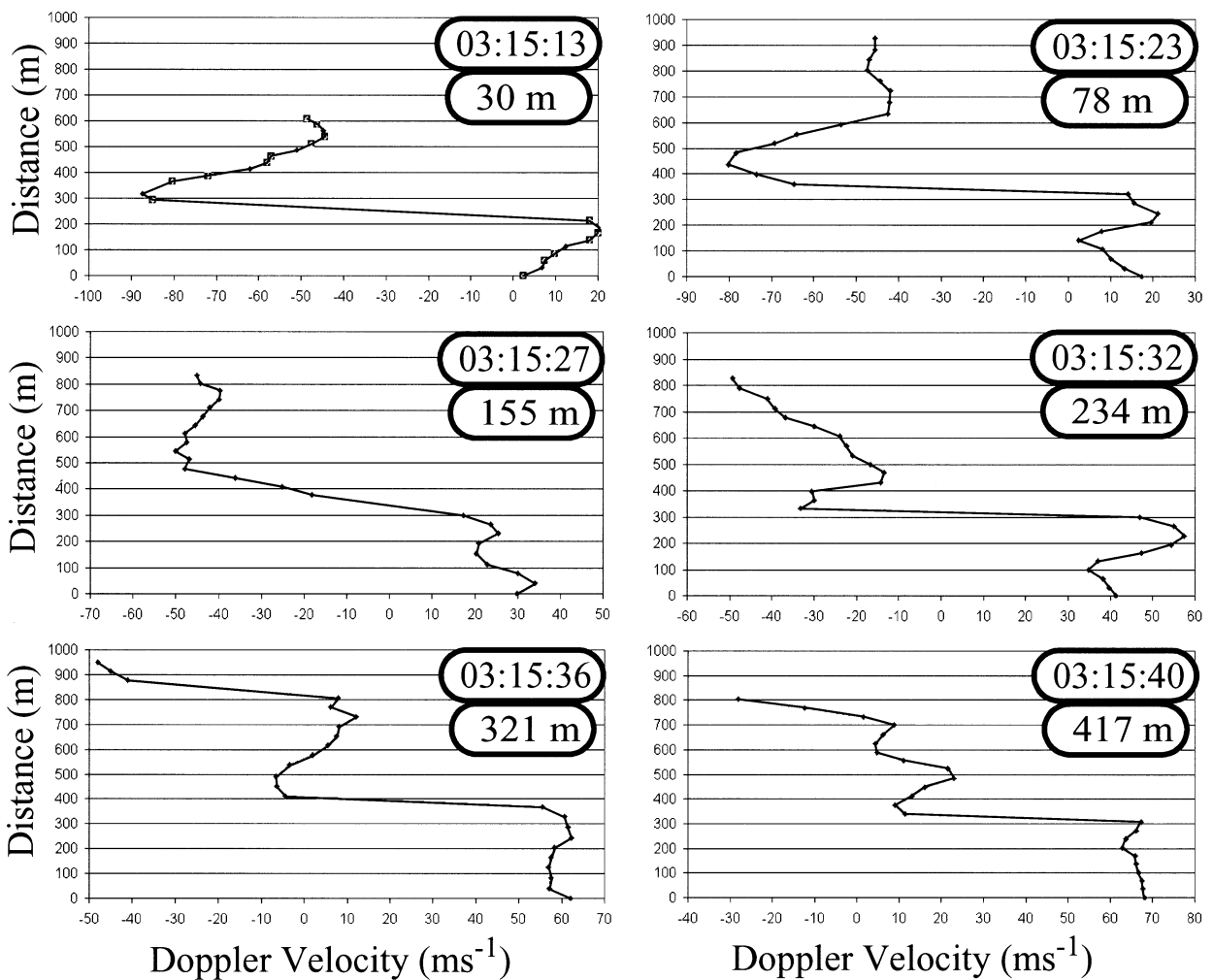

FIG. 12. Doppler velocity cross sections across vortex A at various altitudes. The strong velocity perturbations associated with the vortex were evident in all cross sections. The perturbations were superimposed on the strong gradient of Doppler velocity associated with the tornado (see Fig. 13.). Very strong shear regions were evident at the center of the vortex in most scans with most of the total shear across the vortex occurring across two adjacent radar observations or less than 100 m, despite the fact that the peak perturbations were typically separated by 200–300 m.
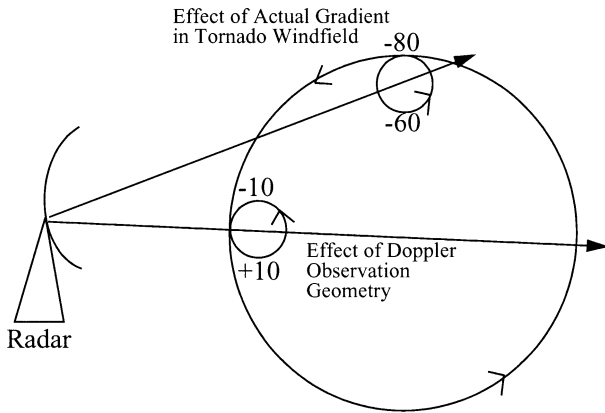
FIG. 13. Two sources of error to ΔV calculations. Even in the absence of velocity perturbations associated with multiple vortices, there would be gradients in the *actual* background tornado velocity field. These would be superimposed on the ΔV calculations to varying degrees depending on the observation geometry. Furthermore, observation geometry could introduce gradients in the observed *Doppler* velocity field in the absence of actual azimuthal wind speed gradients. The worst case is illustrated. Numerical values represent observed Doppler measurements at selected locations in the tornado in the absence of multiple vortices. In this study, only localized regions of intense shear were considered, reducing the chances of false identification. In addition, vortices were considered bona fide only if they were also associated with received power features such as eyes or hooks and were correlated with regions of high spectral width. Tracked vortices exhibited persistent velocity couplets as they revolved about the tornado.

$2\Delta V_r/(R\Delta\Theta)$, where Θ was the azimuth angle of the observations, R was the range to the observation location from the radar, and V_r was the observed Doppler velocity. Because this calculation involved taking differences across just several radar beams, $\Delta\Theta$ was subject to proportionately large errors. Vertical vorticity calculated using measurements across the entire vortex ranged from about 1.0 to 2.6 s^{-1}. These, and other observations presented below, were among the largest ever measured in an intense atmospheric vortex and were several times as high as that calculated across the parent tornado (0.15 s^{-1} average shear implied $\zeta = 0.3$ s^{-1}). This vortex, and others discussed below, exhibited intense beam-to-beam shear at their centers. These intense shear zones were present in most slices through the vortex (Fig. 12). The Doppler velocity changed by 80 m s^{-1} in 0.4° in one sweep, with 60 m s^{-1} over 0.54° and 56 m s^{-1} over 0.6° observed in other sweeps, resulting in estimated ζ of 5.2, 2.8, and 2.2 s^{-1}, respectively. Because the Doppler velocities reported from each beam really reflected a weighted average across a beamwidth larger than the beam sampling intervals, these shear and vorticity values were likely *underestimates* of the true peak shear and ζ in the center of the vortex (Burgess et al. 1993; Wood and Brown 1997).

Power and Doppler velocity measurements at any point were due to the sum of the signals returned from the main radar beam and those returned from scattering from radar-beam sidelobes. It is possible that scattering from sidelobes was important in the relatively clear eyes of the multiple vortices because of the surrounding intense, nearby, high-power rings. When the main radar beam was sampling the comparatively clear eye region of a multiple vortex, the first antenna sidelobes would have been illuminating the high-power ring, about 1.5° away, azimuthally, in either direction. Scattering of the sidelobe energy could have contaminated the signals emanating from the eye. The first radar-beam sidelobes were probably at least 20–23 dB lower in intensity than the main radar beam, so two-way rejection, by the radar antenna, of these signals would be approximately 40–46 dB. If the returned signals from the eye regions were dominated by first sidelobe returns, the values of the returned power in these regions should typically be about 37–43 dB lower than that observed in the surrounding rings, assuming the worst case of perfectly superimposed contamination from the left and right first sidelobes (when the observations in the surrounding rings were not themselves contaminated by the saturation of the radar receiver). The observed differences in returned power values between the eyes and the surrounding rings were typically 10 dB or less even in the most well-defined vortices (see, e.g., Figs. 10g,i,k), disproving this hypothesis. However, it cannot be ruled out that the power returned from all the radar sidelobes, extending both azimuthally and in elevation, could sum to reach the values observed in the eyes. Furthermore, multiple-scattering phenomena could have contaminated observations in the eyes. However, because the velocity signatures from all the energy returned from these sidelobes and multiple-scattering paths would be combined, only repeated pathological combinations would produce the systematic smooth velocity patterns, with single intense shear zones, observed over and over again in the multiple vortices.

No presently conceived mechanism of data contamination can explain the intense shear zones. So, a proposed physical mechanism and vortex structure that may explain these observations is presented below in the discussion near the end of this paper.

The ΔV calculations across the multiple vortices might have suffered further from error due to two factors, illustrated in Fig. 13. First, ΔV of the vortex was superimposed on the *actual* velocity gradient in the parent tornadic flow. This effect was most severe when ΔV of the vortex was measured across locations at significantly different radii from the center of the tornado. Second, the measured ΔV was superimposed on the observed *Doppler* velocity gradient of the parent tornado. This effect was most severe when ΔV was measured in the region of the tornado closest or farthest from the radar, where observing geometry most strongly affected the measured Doppler velocity. Although these errors may have affected the magnitude of the multiple vortex ΔVs presented herein, spuriously increasing them, they should not have had a systematic altitude dependence. Furthermore, the characteristics of the multiple vortices
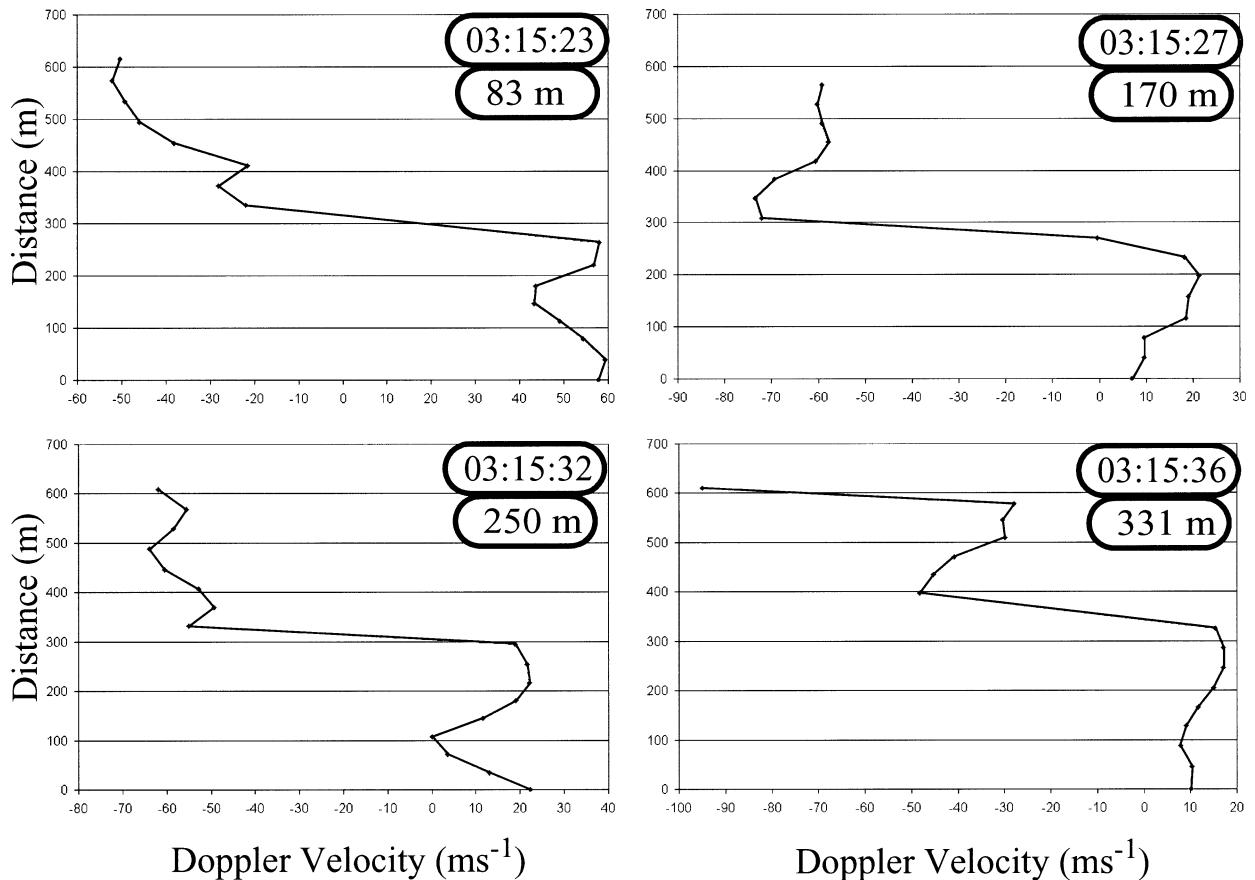
FIG. 14. Doppler velocity cross sections across vortex B at various altitudes; otherwise, same as in Fig. 12.

did not seem to depend on the location relative to the radar, so it is believed that the actual magnitude of the introduced errors was small and did not detract from the presented results.

The translational speed of vortex A was approximately 52 m s^{-1}, with individual calculations based on the velocity and power centers ranging from 33 to 76 m s^{-1} and 8 of 13 calculated values within ± 10 m s^{-1} of the mean. This was about 0.7–0.8 times the V_{atp} (LW) and indicated a propagation velocity upstream at about 0.2–0.3 of V_{atp}, somewhat consistent with predictions of propagation at one-half of the tornado tangential velocity (Ward 1972; Rotunno 1984; Lewellen et al. 1997). Vortex A was observed while it was propagating first perpendicular to, then parallel to, then perpendicular again to the parent tornado translational motion, and the highest observed vortex translational motions were observed, as expected, when the vortex propagation was parallel to the tornado translation. Therefore, average *tornado-relative* propagation speeds were much closer to one-half of the tornado tangential velocity as predicted by theory and experiment. Because upstream tilting of the vortex might have introduced some spurious apparent upstream propagation and because the tornado might

not have been situated exactly in the region containing the maximum flow V_{atp}, these observations might also be consistent with the vortex simply being carried along passively with the background tornadic flow with no upstream propagation (Walko and Gall 1984).

d. Vortices B and B′

Vortex B was tracked for over 40 s starting at 0315: 25.8 UTC. The power and Doppler velocity fields in this vortex are shown along with those of vortex A in Fig. 10. This vortex, outlined with a pink oval, followed a few hundred meters behind vortex A but exhibited some different structural features. It was associated closely with another vortex, titled B′, sometimes appeared as a double vortex, and might have been undergoing vortex breakdown itself.

At 249 m AGL (Fig. 10g) and below, there was a doughnut-with-hole structure at the edge of the main tornado debris region. The surrounding high-power ring had a diameter of 250 m. There was also a hooklike structure 350 m west of the eye, associated with nearby vortex B′, outlined in some sweeps with green ovals. The double vortex structure was most prominent at 332 m AGL with the hook 350 m to the west-northwest of
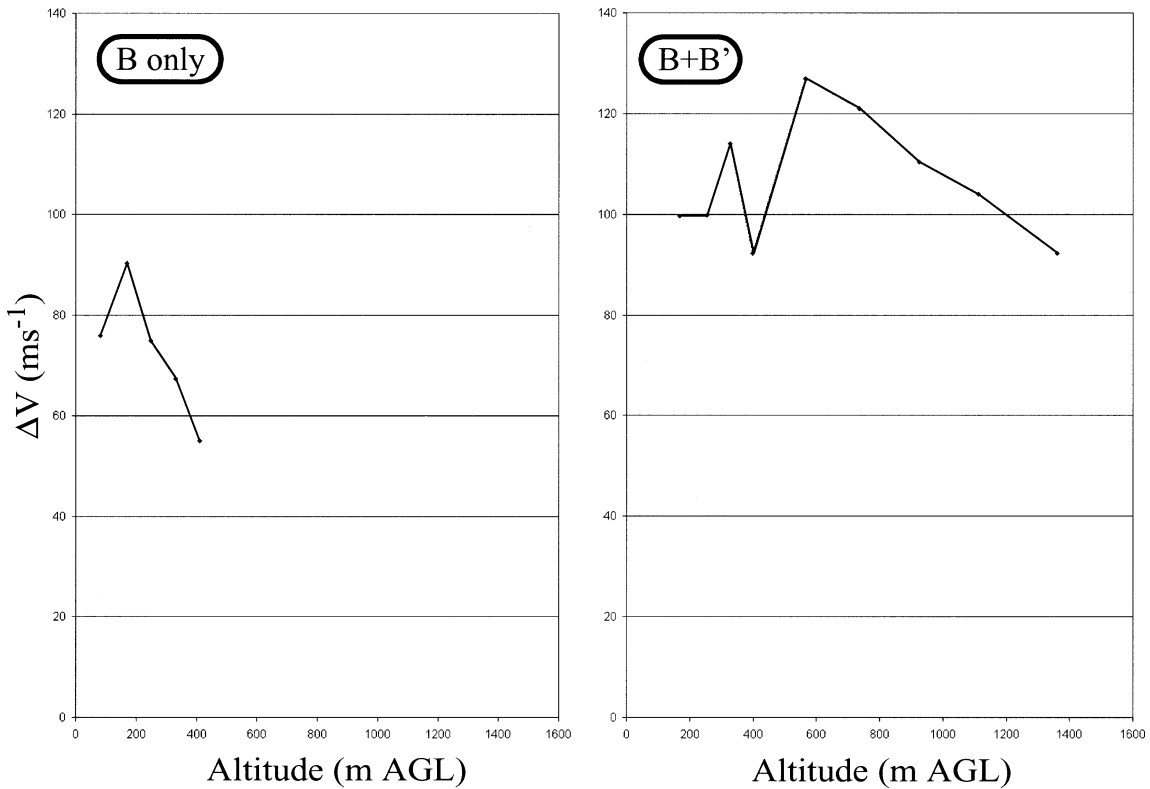
FIG. 15. The ΔV across vortex B and the B + B' combination, as functions of altitude. Values appeared to decrease with altitude in vortex B, but vortices B and B' were difficult to separate above 400 m AGL. When B and B' were taken together, ΔV did not decrease with altitude, but this calculation was particularly sensitive to the factors described in Fig. 13 because of the large combined size of B + B'.

the eye. At 332 and 415 m AGL, B' appears to be embedded in stronger background tornadic flow, and it caught up with B by the time of the observation at 415 m. At higher altitudes, it was difficult to separate the power signatures of vortices B and B', and it is possible that they had combined into one vortex. At 250 m AGL, there was evidence of one or more other vortices behind B', manifested by quasiperiodic high-power protuberances occurring at 300–500-m intervals around the northwest side of the tornado. The spacing of these disturbances implies a wavenumber of approximately 10.

Because of the close proximity of B and B' to each other, ΔV, vorticity, and translational motion calculations were difficult, becoming unreliable above 400 m AGL. Although intense gate-to-gate shears were present in both B and B', with values as high as 76 m s^{-1} over 0.43° (Fig. 14), resulting in azimuthal shear of more than 2 s^{-1} and implying $\zeta > 4$ s^{-1}, the ΔV across the entirety of vortex B was less than the ΔV across vortex A at 248 m AGL and below (Fig. 15, left). However, the combined ΔV across B + B' was higher (Fig. 15, right), exceeding 120 m s^{-1} in some sweeps. The combined ΔV did not exhibit the decrease with altitude observed in vortex A or B alone, except above 600 m. These combined ΔV calculations might have suffered especially from the errors described in Fig. 13, however.

As suggested by the power fields, it is possible that B and B' had combined into a single vortex above 500 m or were, at a minimum, inseparable using the current data. Estimated translational motion was about 20 m s^{-1} at low levels for B and about 40–50 m s^{-1} for B', both significantly slower than V_{atp}—this despite the fact that they were moving perpendicular and then parallel to the tornado translational motion.

e. Vortex C

Vortex C was observed between 159 and 883 m AGL, from 0314:29.5 through 0314:55.6 UTC (Fig. 16). Above 883 m, the vortex was either too weak to detect or had merged with other vortices. The vortex was characterized by a nearly enclosed hook in the power structure at 159 m AGL, and a doughnut-with-hole structure above. The prominent eye was easily pinpointed and moved with an apparent translational velocity of 45–60 m s^{-1}, between 0.6 and 0.9 of V_{atp} at that time. Tornado-relative velocities were close to $0.5V_{\text{atp}}$. Again, the location of the vortex relative to the region of V_{atp}, and the possible effects of helical tilting, make these results also consistent with no upstream propagation.

The velocity signature of the vortex appeared to be less intense than vortex A or the combination of B and
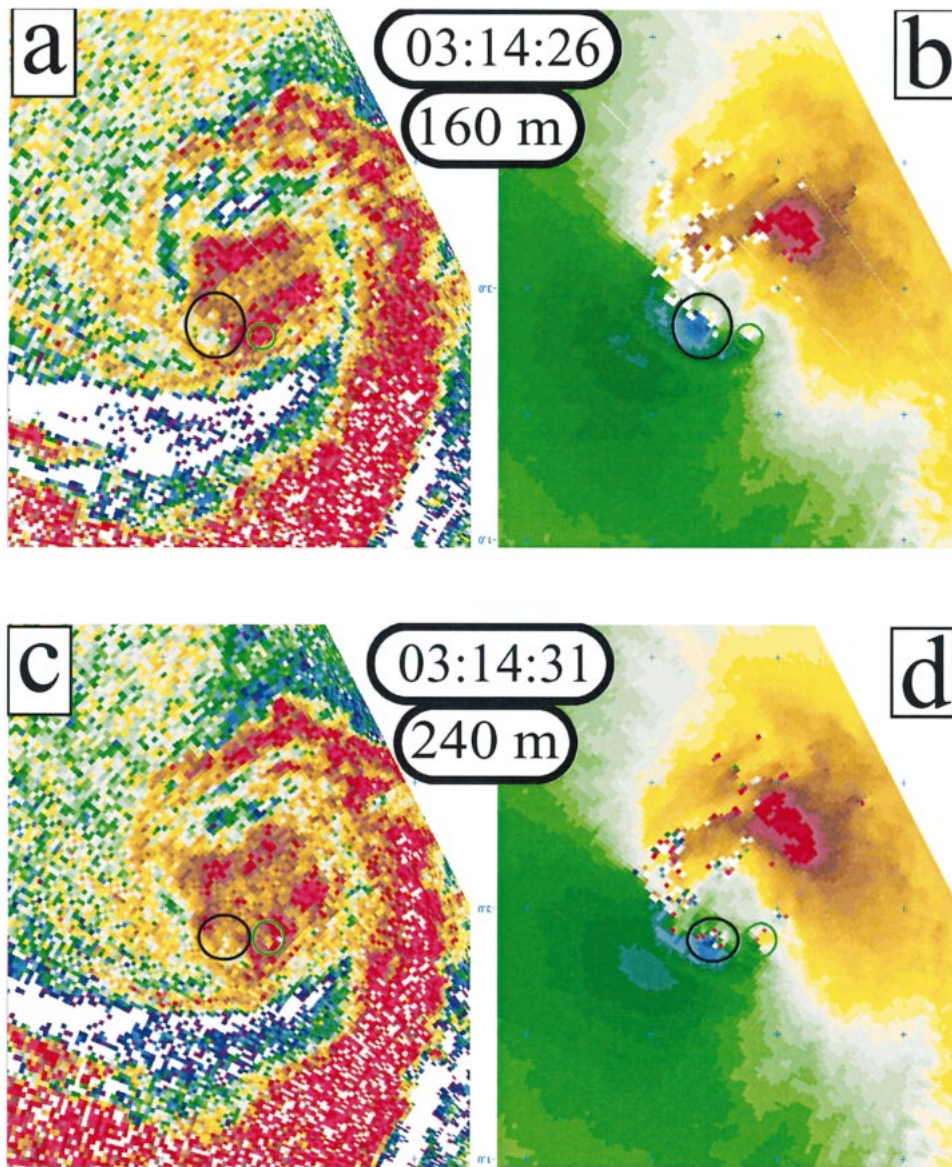
FIG. 16. Tracking multiple vortex C. Otherwise the same as in Fig. 10. Vortex C is indicated with a black ellipse. Other less trackable vortices are indicated with green ellipses.

B′, with ΔV values decreasing with increasing altitude from 86 m s^{-1} at 159 m AGL to about 60 m s^{-1} at 883 m AGL (Fig. 17). As with the other vortices, intense shear existed at the core, with estimated vertical vorticity values ranging up to 2–3 s^{-1}, whereas values across the entire vortex were more typically 0.9–1.6 s^{-1}.

f. Vortex D

Vortex D was first detected at the lowest observed levels on the south side of the tornado. The Doppler velocity fields in this vortex at 0313:11.6, 0313:16.1, and 0313:20.1 UTC at 70, 140, 202, and 262 m AGL

are presented in Fig. 18. The vortex was never distinct in the power field (not shown) and could not be identified in higher-altitude sweeps. The center of the vortex was inside the core radius of the main tornado, more consistent with the predictions of Llewellen et al. (1997). The translation velocity of the vortex, based on only two reliable calculations, was 55 m s^{-1}, but this likely contained a significant component of tornado translation motion, so the speed relative to the tornado was approximately 45 m s^{-1}, about $0.7V_{\text{atp}}$ at that time.

The ΔV across the vortex at 70 m AGL was 95 m s^{-1}, with a peak absolute Doppler velocity, the highest measured at any time in this tornado, of -109.5 m s^{-1},
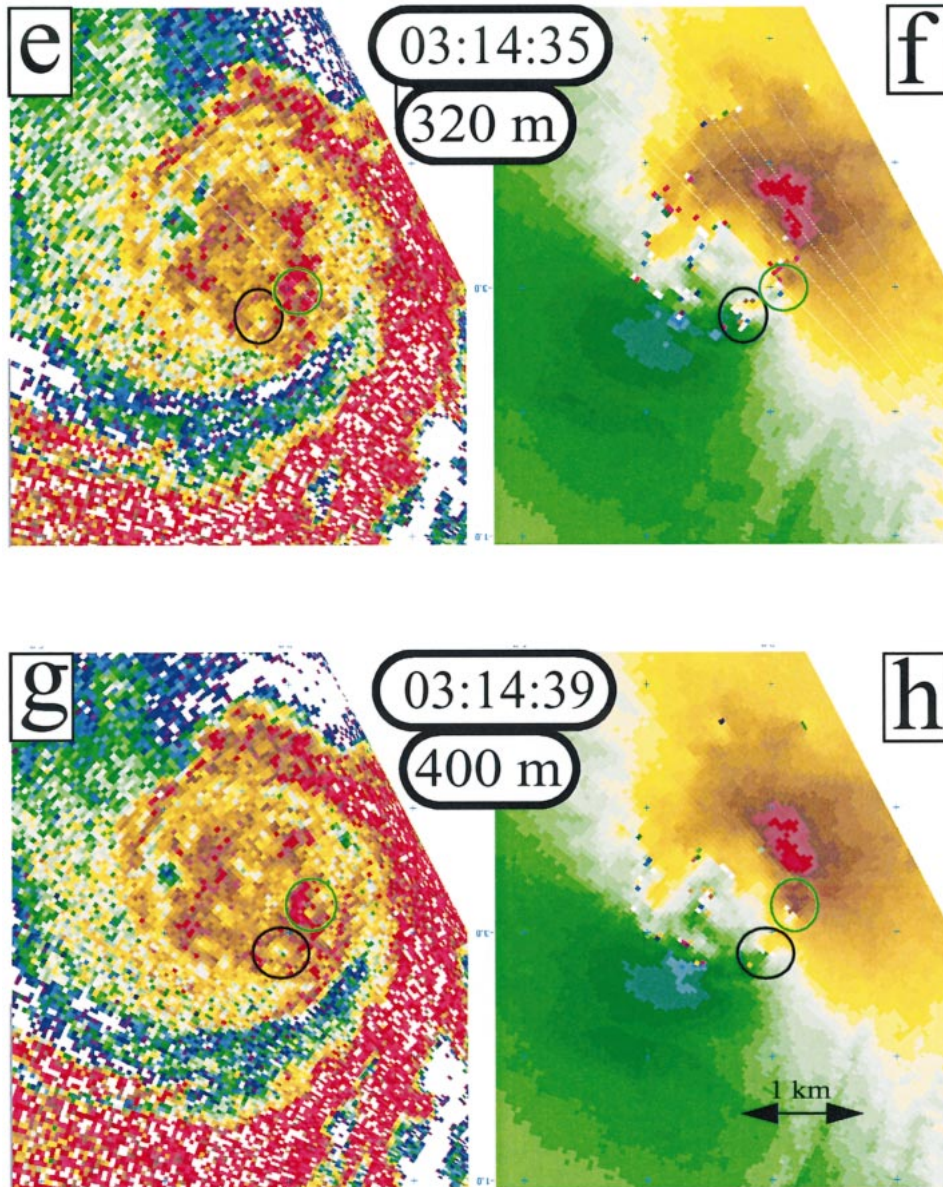
FIG. 16. (*Continued*)

which was about $1.5V_{atp}$. Azimuthal shear across the vortex, depending on the measurement location, varied from 95 m s^{-1} over 3° to 89 m s^{-1} over 1.7° and to 92.5 m s^{-1} over 1.1°. This result implied $\zeta = 0.9$–1.4 s^{-1} over the entire vortex, with $\zeta = 2.3$ s^{-1} in the peak shear region near the center.

The vortex weakened with height, and the ΔV values were only 68 m s^{-1} at 140 m AGL and 60 m s^{-1} at 202 m AGL. Vertical vorticity measured across the entire vortex was lower, with $\zeta = 0.7$ and 0.9 s^{-1} at 140 and 202 m AGL, respectively. Vertical vorticity calculated from beam-to-beam shear was as high as 3.4 s^{-1} aloft.

g. Other, less trackable, multiple vortices

Several other multiple vortices were observed but were not unambiguously trackable over several radar sweeps. One low-altitude radar sweep at 0316:38 UTC (Fig. 19) illustrates several of these transient vortices. Some of these vortices were very intense, with ΔVs of nearly 100 m s^{-1} near the ground. They typically appeared to be smaller than the large trackable vortices. Trackability might have been a function of vortex longevity and the DOW's ability to resolve unambiguously, and to separate, smaller vortices from each other. At 0316:38 UTC, the six resolvable vortices appeared only
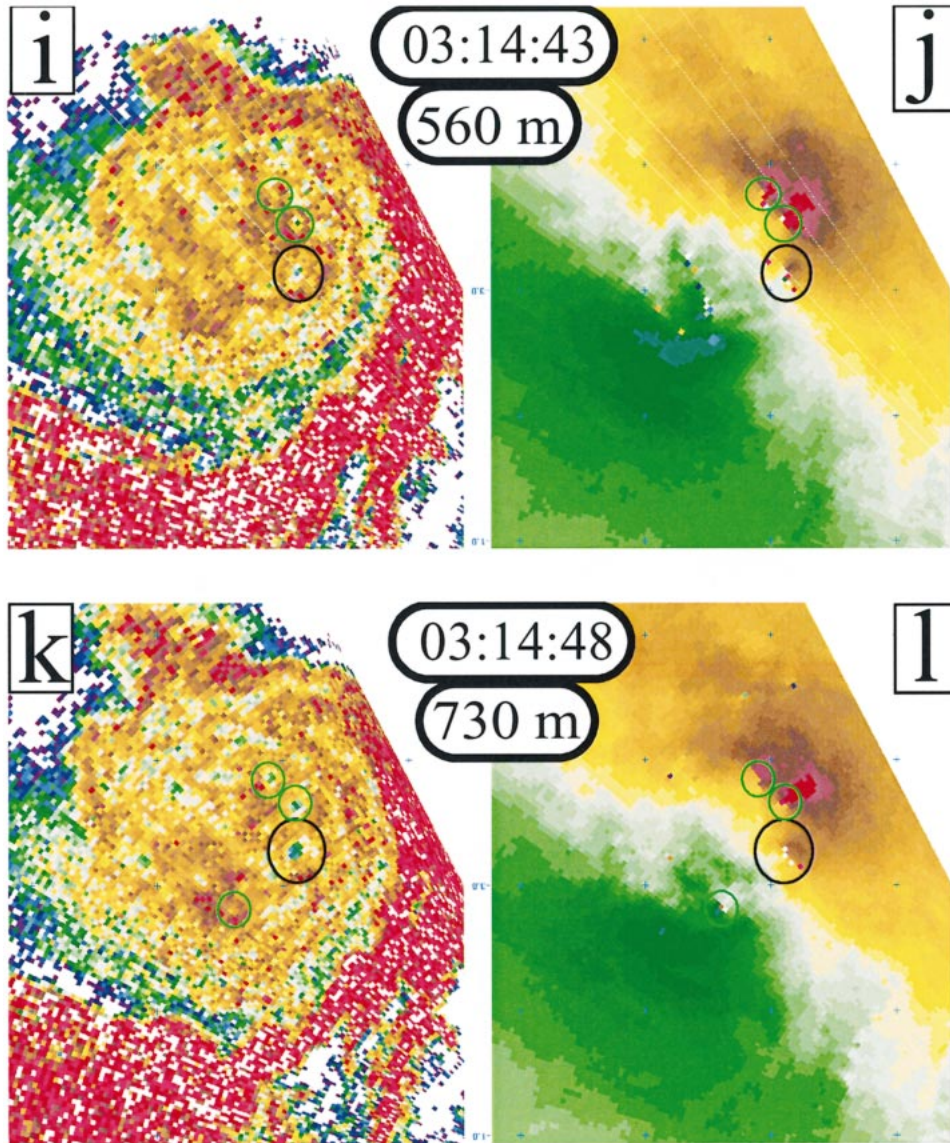
FIG. 16. (*Continued*)

on the western side of the tornado. The apparent wavenumber of the vortices on that side was about 10, however. This represents a higher value than that observed in laboratory or computer simulations (Rotunno 1984; Walko and Gall 1984). Lee and Wurman (2001) report swirl ratios in this tornado of approximately 1–5 during the observation period.

h. Anticyclonic vortices and intense shear zones well away from the tornado center

Over 1.5 km from the center of the tornado, well outside the region of maximum winds, intense anticyclonic shear zones (not shown), possibly associated with vortices, were present. The velocity perturbations associated with these anticyclonic vortices were less intense, ranging up to about 60 m s^{-1}, but were still significant. Intense gate-to-gate shear implied small regions with vertical vorticity of approximately -2 s^{-1}, comparable to or less than that observed in the cyclonic vortices nearer the center of circulation. Some of the anticyclonic vortices were also associated with low-power eyes as they rotated around the tornado. Some of these are visible in Figs. 7, 10, and elsewhere, but they are not the focus of this paper.

i. Expected surface conditions during tornado and multiple-vortex passages

Because the translational velocity and structure of the wind field of both the primary tornado and its multiple vortices were resolved well, it was possible to conduct
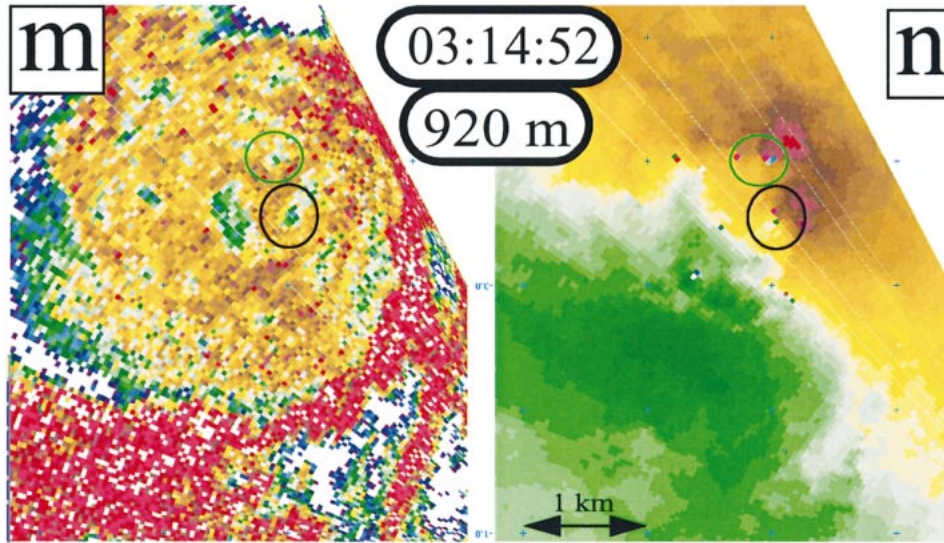
FIG. 16. (*Continued*)

a space–time conversion to estimate what a hypothetical stationary observer would have experienced during the tornado and multiple-vortex passages. Because the radar beamwidth was about 75 m at the range of the center of the tornado, the estimated ''surface'' conditions dis-

cussed below best describe conditions about 30 m AGL, depending, of course, on the exact topography near the observer.

In the absence of multiple vortices, an observer in the path of the center of the eye would have experienced a gradual increase in wind speed, from 30 to 40 m s^{-1} in 45–60 s, then from 40 to 50 m s^{-1} during the next 35–45 s (Fig. 8). Winds would have increased rapidly to approximately 80 m s^{-1} over the next 35 s. Any observer still standing would then have observed winds that rapidly decreased at a nearly linear rate to below 30 m s^{-1}, continued to decrease, then changed direction, then increased to over 30 m s^{-1}, and then increased to 80 m s^{-1} on the lee side of the circulation's core flow region. An observer in the path of the exact center of the tornado would have experienced a 30-s period of winds below 30 m s^{-1} during the passage of the core flow region or eye of the tornado. Depending on which regions of particular multiple vortices that an observer experienced, winds in excess of 50 m s^{-1} would have lasted from as little as 35 s to as much as 75 s. Peak instantaneous wind speeds would have ranged from 80 to near 110 m s^{-1}, perhaps higher. Winds in excess of 70 m s^{-1} could have been experienced for 20 s or more. Winds over 100 m s^{-1} only existed over one to three contiguous radar gates, implying that they represented wind gusts with durations of perhaps 1–2 s. Observers who were approximately 600–800 m to the east or southeast of the center of the path of the tornado would have experienced the longest and most severe conditions as the region of maximum winds passed overhead, possibly over 70 m s^{-1} or more for up to 60 s. The *long duration* of extremely high wind speeds would certainly *exacerbate* surface damage. The town of Mulhall, Oklahoma, was on the northwest, or least windy, side of the path of the tornado (Fig. 5). The town center was
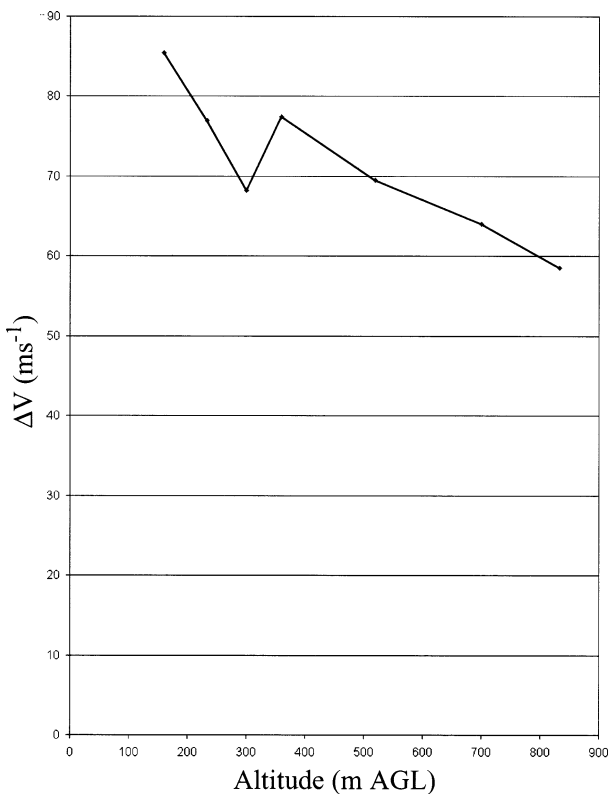

FIG. 17. Doppler velocity difference ΔV across vortex C as a function of altitude. The ΔV was about 86 m s^{-1} near the ground and decreased with increasing altitude.
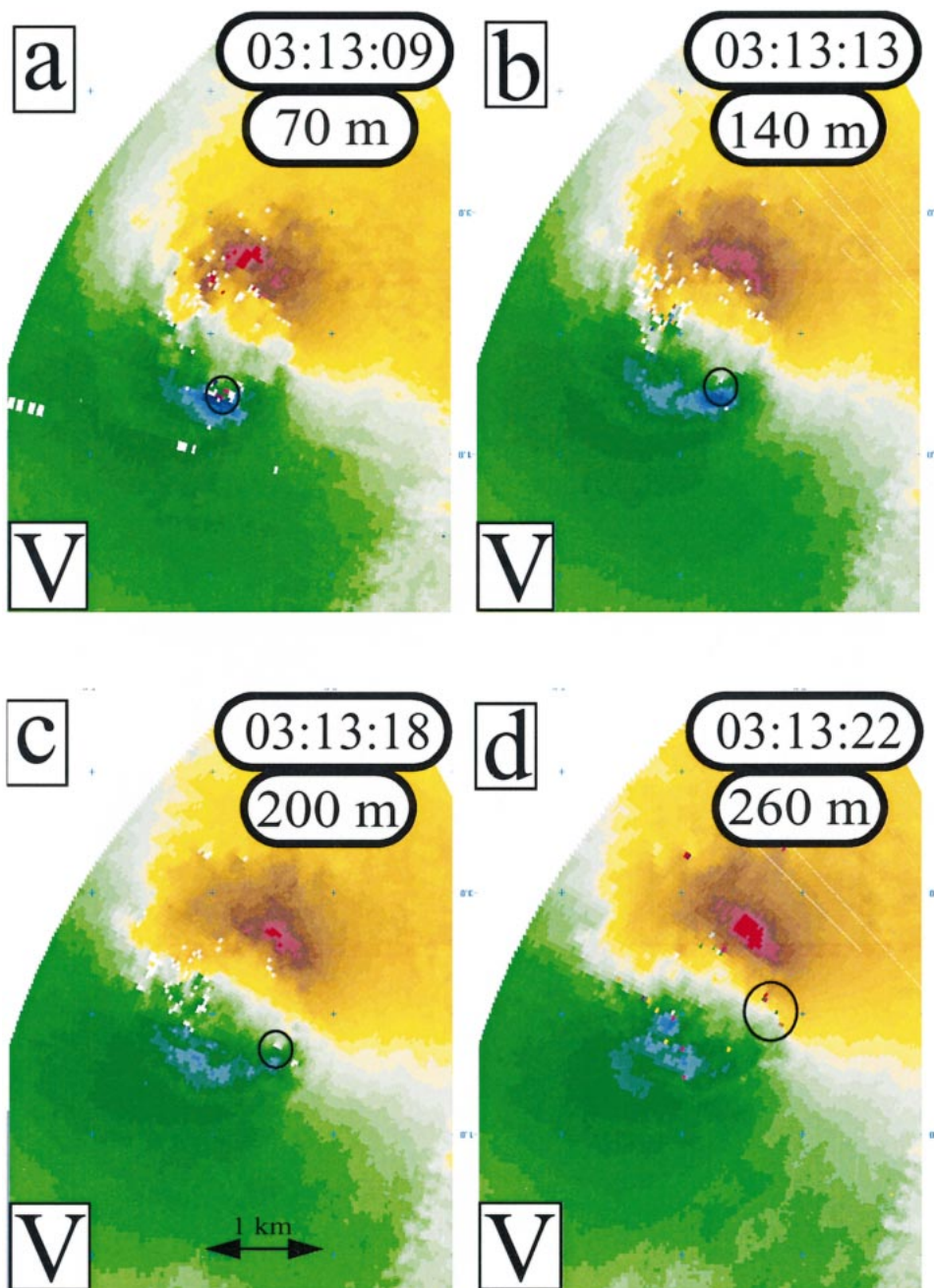
FIG. 18. Tracking vortex D. *Doppler velocity only* in four scans through vortex; otherwise, the same as in Fig. 10. Vortex D is indicated with a black ellipse as it revolved around the south of the tornado. It was difficult to discern after 0313:22 UTC.

a few hundred meters away from the region of peak winds, but the southeast side of town was grazed by the northwest edge of the core flow region and probably suffered the effects of winds in excess of 80 m s^{-1}.

If the observer had been unfortunate enough to have been impacted by the central high-shear portion of one of the multiple vortices, the experienced wind velocity would have changed by over 50 m s^{-1} in less than 1 s.

This would have represented an observed acceleration of over 50 m s^{-2}, or over 5 times the acceleration of gravity g. This was probably the most intense wind velocity change ever calculated in an observed macroscale meteorological phenomenon and might have had a profound impact on structures. It is likely that the motion of large debris would have differed significantly from the motion of air parcels in this environment. *Av-*
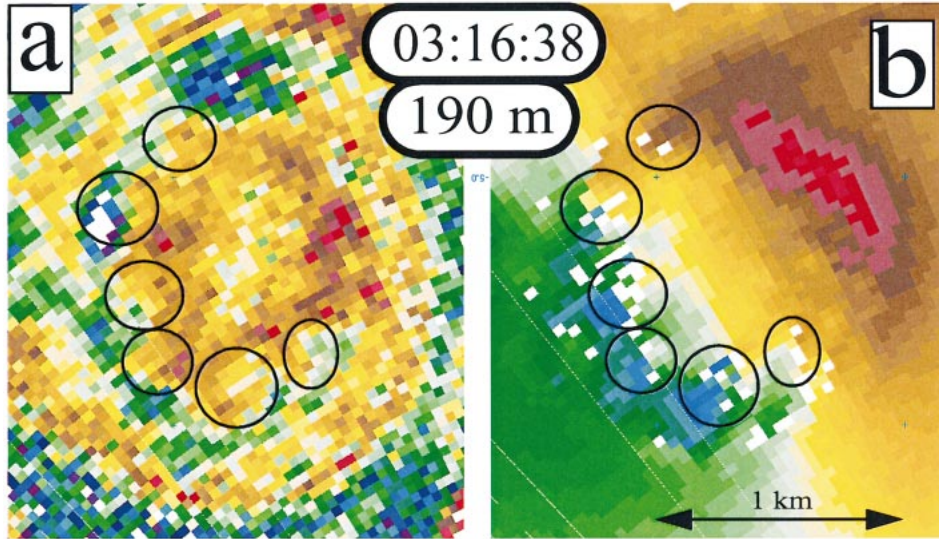
FIG. 19. (a) Power and (b) Doppler velocity fields in the tornado illustrating a train of quasiperiodic multiple vortices with high wavenumber. Otherwise, the same as in Fig. 10. Miniature hook echoes and waves in the outer edge of the debris cloud and intense shear zones demarked at least six multiple vortices on the western side of the tornado and are indicated with black ellipses. Note change of scale in this figure.

erage wind velocity changes in the multiple vortices would have been comparatively much more gradual, with 100 m s^{-1} changes occurring over about 5 s (20 m s^{-2} = 2g) as 250-m-diameter vortices passed over particular locations at translational velocities of about 50 m s^{-1}. Of course, the exact temporal variation of experienced wind speed would have depended strongly on the exact location of the observer relative to individual vortices. It would have been possible that observers in fortunate locations would have never experienced the peak winds of the tornado, because the passage of a well-timed multiple vortex could have partially canceled peak winds as the core radius of the primary tornadic circulation passed overhead. Without dual-

FIG. 20. Cross section through inferred tangential (V_t) and hypothesized vertical (W) wind field in the multiple vortices observed in this tornado. The wind field structure of the observed multiple vortices differed significantly from that of observed tornadic circulations and idealized vortices. The observed multiple vortices exhibit narrow regions containing approximately one-half of the total change in V_t. This is in sharp contrast to either well-resolved or poorly resolved solid-body rotation in tornadoes (see Fig. 8).

Doppler vector wind observations it was impossible to quantify this effect, but paths through the tornado could be traced in which peak Doppler velocities never exceed 60 m s^{-1} (Fig. 19). Although winds of 60 m s^{-1} would be potentially damaging, this potential would be considerably less than that of the >100 m s^{-1} winds that could have been experienced in different but nearby paths, especially given that the ability of winds to cause damage increases as at least the square of the velocity.

5. Discussion

Doppler velocity, power, and spectral-width radar observations presented herein permit the characterization of the multiple-vortex structure of this exceptionally large and powerful tornado. The velocity structure of these vortices differs significantly from that of tornadoes. Large tornadoes have been observed to contain a core flow region exhibiting approximately solid-body rotation with $V \propto R$ surrounded by a region in which the wind decreased at approximately $V \propto R^{-0.5}$–$V \propto R^{-0.6}$ (see Fig. 8. and WG), though sometimes the outer region was characterized by multiple wind field maxima. When the aspect ratio (Wood and Brown 1997) of the observations was small, however, extreme gate-to-gate shears with correspondingly extreme shear and implied vertical vorticity values were not observed because the observed core flow region separated the regions of extreme inbound and outbound velocities.

The multiple vortices observed in this tornado exhibited extremely high shear and implied high vertical vorticity at their centers. Frequently, these regions contained one-half or more of the total shear observed across the vortices (Figs. 12 and 14) and vertical vor-
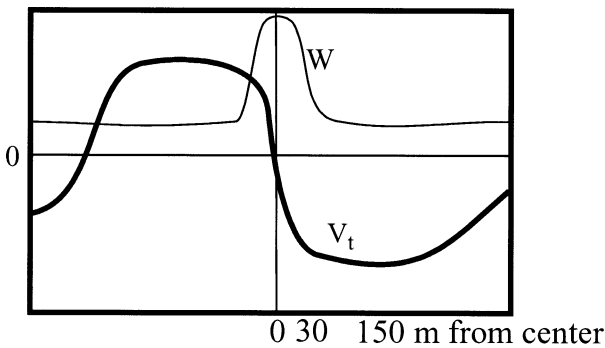
Narrow Intense Updraft

Maximum Tangential Winds and ring of debris

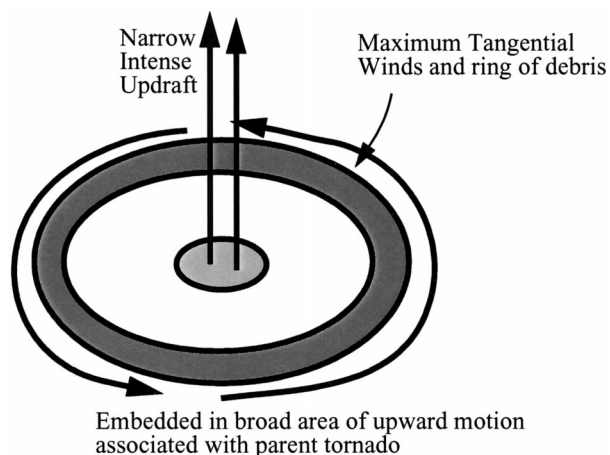Embedded in broad area of upward motion associated with parent tornado

FIG. 21. Schematic illustration of the hypothesized velocity and power structure of the multiple vortices observed in this tornado. The rings of debris were centrifuged from the center of the vortices in the presence of perhaps slight upward motion (see Fig. 20) possibly associated with the parent tornado. An intense, very narrow, updraft was associated with convergence and the strong gate-to-gate observed shear at the center of the vortices.

ticity of several inverse seconds. The inferred tangential velocity structures (Fig. 20) were very different than that predicted by an ideally sampled or poorly sampled combined Rankine vortex (Wood and Brown 1997).

It is proposed that intense and horizontally very narrow (<40 m) transient updrafts existed in the center of these vortices (Figs. 20 and 21). This would have caused intense but transient horizontal convergence and resultant stretching of vorticity near the center of the vortices. It is hypothesized that the transient and narrow characteristics of the updrafts and/or the rapid passage, at translational velocities of approximately 50 m s^{-1}, of the small updrafts through particular regions of the tornado did not allow the air in the vortices to adjust to states that exhibited the solid-body rotation observed in this or other large tornadoes. Thus, comparatively high angular-momentum air (as compared with what would occur in solid-body rotation) reached close to the centers of the vortices.

It was observed that the vortices revolved about the tornado at less than V_{atp}, the peak azimuthally averaged tangential wind velocity. Rossby-type waves in the intense vorticity gradient of the tornado would be expected to propagate upstream and to translate at less than the background wind speed. Because the implied wavelength of the observed vortices was short and there were significant uncertainties in their translational velocity, the Rossby-type mechanism could not be excluded. Instability mechanisms and energy budgets of multiple vortices have been discussed in detail in Gall (1983), Walko and Gall (1984), Rotunno (1984), and elsewhere and cannot be evaluated with the observations presented herein. The propagation speed of the vortices of near $0.5V_{atp}$, as well as their velocity amplitude that produced peak values of about $1.5V_{atp}$, were consistent

with some numerical and laboratory predictions and contradicted others. However, it is important to note that the vortices may have been moving slower than V_{atp} but may not be located at the radius of V_{atp} and may therefore be exhibiting no upstream propagation, consistent with Walko and Gall (1984).

The rapid motion and small scale of these observed vortices draw attention to the need for volumetric observations at much shorter time intervals. Many of the ambiguities in the current study concerning the estimation of the propagation speed of the vortices around the tornado and measurement of tilting with height could be addressed with nearly simultaneous observations at all altitudes. A rapid-scan mobile radar system that can obtain such observations using multiple beams and is capable of completing 6–12 sweep volume scans in less than 6–10 s is under construction (Wurman and Randall 2001) and will provide the opportunity to resolve multiple-vortex structure and evolution better, beginning in about 2003.

REFERENCES

Agee, E. M., C. Church, C. Morris, and J. Snow, 1975: Some synoptic aspects and dynamic features of vortices associated with the tornado outbreak of 3 April 1974. *Mon. Wea. Rev.,* **103,** 318–333.
——, J. T. Snow, F. S. Nickerson, P. R. Clare, C. R. Church, and L. A. Schaal, 1977: An observational study of the West Lafayette, Indiana, tornado of 20 March 1976. *Mon. Wea. Rev.,* **105,** 893–907.
Bluestein, H. B., and A. L. Pazmany, 2000: Observations of tornadoes and other convective phenomena with a mobile, 3-mm wavelength, Doppler radar: The spring 1999 field experiment. *Bull. Amer. Meteor. Soc.,* **81,** 2939–2951.
——, J. G. LaDue, H. Stein, D. Speheger, and W. P. Unruh, 1993: Doppler radar wind spectra of supercell tornadoes. *Mon. Wea. Rev.,* **121,** 2200–2221.
——, A. L. Pazmany, J. C. Galloway, and R. E. McIntosh, 1995: Studies of the substructure of severe convective storms using a

mobile 3-mm-wavelength Doppler radar. *Bull. Amer. Meteor. Soc.,* **76,** 2155–2169.

Burgers, J. M., 1948: A mathematical model illustrating the theory of turbulence. *Advances in Applied Mechanics,* R. von Mises and T. von Kármán, Eds., Academic Press, 171–199.

Burgess, D. W., R. J. Donaldson Jr., and P. R. Desrochers, 1993: Tornado detection and warning by Radar. *The Tornado: Its Structure, Dynamics, Prediction and Hazards, Geophys. Monogr.,* No. 79, Amer. Geophys. Union, 203–221.

——, M. A. Magsig, J. Wurman, D. C. Dowell, and Y. Richardson, 2002: Radar observations of the 3 May 1999 Oklahoma City tornado. *Wea. Forecasting,* **17,** 456–471.

Carbone, R. E., M. J. Carpenter, and C. D. Burghart, 1985: Doppler radar sampling limitations in convective storms. *J. Atmos. Oceanic Technol.,* **2,** 357–361.

Church, C. R., and J. T. Snow, 1993: Laboratory models of tornadoes. *The Tornado: Its Structure, Dynamics, Prediction and Hazards, Geophys. Monogr.,* No. 79, Amer. Geophys. Union, 19–39.

——, J. T. Snow, G. L. Baker, and E. M. Agee, 1979: Characteristics of tornado-like vortices as a function of swirl ratio: A laboratory investigation. *J. Atmos. Sci.,* **36,** 1755–1776.

Davies-Jones, R. P., 1976: Laboratory simulations of tornadoes. *Proc. Symp. on Tornadoes: Assessment of Knowledge and Implications for Man,* Boston, MA, Amer. Meteor. Soc., 151–174.

Dowell, D. C., J. Wurman, and L. Wicker, 2001: Centrifuging of scatterers in tornadoes. Preprints, *30th Conf. on Radar Meteorology,* Munich, Germany, Amer. Meteor. Soc., 307–309.

Fiedler, B. H., 1998: Wind-speed limits in numerically simulated tornadoes with suction vortices. *Quart. J. Roy. Meteor. Soc.,* **124,** 2377–2392.

——, and R. Rotunno, 1986: A theory for the maximum windspeeds in tornado-like vortices. *J. Atmos. Sci.,* **43,** 2328–2340.

Fujita, T. T., 1970: The Lubbock tornadoes: A study of suction spots. *Weatherwise,* **23,** 160–173.

Gall, R. L., 1983: A linear analysis of the multiple vortex phenomenon in simulated tornadoes. *J. Atmos. Sci.,* **40,** 2010–2024.

Lee, W. C., and J. Wurman, 2001: Evolution and structure of a tornado during the 4 May 1999 tornado outbreak near Oklahoma City. Preprints, *30th Conf. on Radar Meteorology,* Munich, Germany, Amer. Meteor. Soc., 304–306.

Lewellen, W. S., 1993: Tornado vortex theory. *The Tornado: Its Structure, Dynamics, Prediction and Hazards, Geophys. Monogr.,* No. 79, Amer. Geophys. Union, 19–39.

——, D. C. Lewellen, and R. I. Sykes, 1997: Large-eddy simulation of a tornado's interaction with the surface. *J. Atmos. Sci.,* **54,** 581–605.

Pauley, R. L., and J. T. Snow, 1988: On the kinematics and dynamics of the 18 July 1986 Minneapolis tornado. *Mon. Wea. Rev.,* **116,** 2732–2736.

Richardson, P. Y., D. C. Dowell, and J. Wurman, 2001: Preliminary high-resolution dual-Doppler analyses of two tornadic thunderstorms. Preprints, *30th International Conf. on Radar Meteorology,* Munich, Germany, Amer. Meteor. Soc., 295–297.

Rott, N., 1959: On the viscous core of a line vortex. *J. Appl. Math. Phys.,* **9B,** 543–553.

Rotunno, R., 1977: Numerical simulation of a laboratory vortex. *J. Atmos. Sci.,* **34,** 1942–1956.

——, 1978: A note on the stability of a cylindrical vortex sheet. *J. Fluid Mech.,* **87,** 761–771.

——, 1979: A study in tornado-like vortex dynamics. *J. Atmos. Sci.,* **36,** 140–155.

——, 1984: An investigation of a three-dimensional asymmetric vortex. *J. Atmos. Sci.,* **41,** 283–298.

Snow, J. T., 1978: On inertial instability as related to the multiple-vortex phenomenon. *J. Atmos. Sci.,* **35,** 1660–1677.

Staley, D. O., and R. L. Gall, 1979: Barotropic instability in a tornado vortex. *J. Atmos. Sci.,* **36,** 973–981.

Speheger, D. A., C. A. Doswell III, and G. J. Stumpf, 2002: The tornadoes of 3 May 1999: Event verification in central Oklahoma and related issues. *Wea. Forecasting,* **17,** 362–381.

Walko, R., and R. Gall, 1984: A two-dimensional linear stability analysis of the multiple vortex phenomenon. *J. Atmos. Sci.,* **41,** 3456–3471.

Ward, N. B., 1972: The exploration of certain features of tornado dynamics using a laboratory model. *J. Atmos. Sci.,* **29,** 1194–1204.

Wood, V. T., and R. A. Brown, 1997: Effects of radar sampling on single-Doppler velocity signatures of mesocyclones and tornadoes. *Wea. Forecasting,* **12,** 928–938.

——, and ——, 2000: Oscillations in mesocyclone signatures with range owing to azimuthal radar sampling. *J. Atmos. Oceanic Technol.,* **17,** 90–95.

Wurman, J., 1999: Preliminary results from the Radar Observations of Tornadoes and Thunderstorm Experiment (ROTATE-98/99). Preprints, *29th Conf. on Radar Meteorology,* Montreal, QC, Canada, Amer. Meteor. Soc., 613–616.

——, 2001: The DOW mobile multiple-Doppler network. Preprints, *30th Conf. on Radar Meteorology,* Munich, Germany, Amer. Meteor. Soc., 95–97.

——, and S. Gill, 2000: Finescale radar observations of the Dimmitt, Texas (2 June 1995), tornado. *Mon. Wea. Rev.,* **128,** 2135–2164.

——, and M. Randall, 2001: An inexpensive, mobile, rapid-scan radar. Preprints, *30th International Conf. on Radar Meteorology,* Munich, Germany, Amer. Meteor. Soc., 98–100.

——, J. M. Straka, and E. N. Rasmussen, 1996a: Preliminary radar observations of the structure of tornadoes. Preprints, *18th Conf. on Severe Storms,* San Francisco, CA, Amer. Meteor. Soc., 17–22.

——, ——, and ——, 1996b: Fine-scale Doppler radar observations of tornadoes. *Science,* **272,** 1774–1777.

——, ——, ——, M. Randall, and A. Zahrai, 1997: Design and deployment of a portable, pencil-beam, pulsed, 3-cm Doppler radar. *J. Atmos. Oceanic Technol.,* **14,** 1502–1512.

Zrnić, D. S., and R. J. Doviak, 1975: Velocity spectra of vortices scanned with a pulse-Doppler radar. *J. Appl. Meteor.,* **14,** 1531–1539.